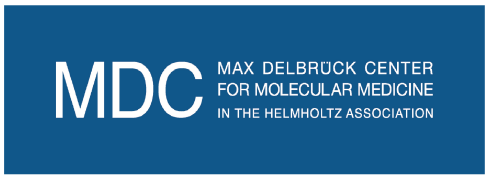

Freie Universität Berlin
Max-Delbrück-Centrum für Molekulare Medizin

Spectroscopic and biophysical characterization of novel fluorescent drug analogues

by

Jagannath Satpathy

A thesis submitted in partial fulfilment of the requirements for the degree of Master of Science in Physics

Department of Physics
Freie Universität Berlin

Thesis Supervisors:

Dr. Paolo Annibale
Prof. Dr. Joachim Heberle
Priv.-Doz. Dr. Michael Haumann

July 6, 2022

Spectroscopic and biophysical characteization of novel fluorescent drug analogues

Master's Thesis

Author: Jagannath Satpathy

Submission Date: July 6, 2022

Thesis Supervisors

Dr. Paolo Annibale
Receptor Signaling Lab
Max-Delbrück-Centrum für Molekulare Medizin (MDC)

Prof. Dr. Joachim Heberle
Institute of Experimental Physics
Experimental Molecular Biophysics
Freie Universität Berlin

Priv.-Doz. Dr. Michael Haumann
Department of Physics
Freie Universität Berlin

Spectroscopic and biophysical characterization of novel fluorescent drug analogues

ABSTRACT

Since the pioneering work of Herschel in 1820, fluorescence spectroscopy and microscopy have been the most informative and sensitive techniques and are widely used to characterize biomolecular functions. This thesis presents the methodology and application of different fluorescent spectroscopy techniques to characterize the novel fluorescent drug analogues. Fluorescence-based drug analogues have played a key role in understanding the functionality of cell receptors and their associated signaling complexes at a molecular level. Fluorescent drug analogues are the building block of biological macromolecules used to understand the complexity of the cell membrane and signaling. Our study aims to determine the behaviour of novel drugs by exploiting the properties of fluorescent analogs.

The Receptor Signaling Group at the MDC-Berlin recently displayed how to use 8-FDA-cAMP, a Fluorescein Diacetate (FDA)-conjugate of cAMP, a key cell 2nd messenger, to study its intracellular dynamics. Here we studied two drug analogues generated based upon the same principle of FDA-conjugation. Highly sensitive Time Correlated Single Photon Counting (TCSPC) and confocal laser scanning microscopy were employed to characterize the novel fluorescent drug analogues. In this thesis, the construction and demonstration of TCSPC, UV-Vis spectrophotometer and a laser scanning confocal microscope setup have been explained.

Moreover, the cellular uptake and subcellular import kinetics behaviour of 8-FDA-cAMP, MAN193, and AG3457 fluorescent molecules were investigated using FDA as a control. The subcellular localization in the region of mitochondria was observed and analyzed for MAN193 and 8-FDA-cAMP molecules, although no subcellular localization was observed for the AG3457 molecule. A competition binding experiment was employed to understand the behaviour of cellular uptake with or without preincubation with a competitor binding molecule. We further characterized the effect of dimethyl sulfoxide (DMSO) on the membrane permeability of FDA and 8-FDA-cAMP molecules by measuring the cellular uptake kinetics on HEK293T cells.

Acknowledgements

I would like to acknowledge Freie Universität Berlin for giving me the opportunity to study in this program: it was a wonderful experience indeed!

First, I would like to thank my supervisor Dr. Paolo Annibale for his scientific guidance, helpful advice, for providing me such interesting topic and making this thesis a success, it would not have been possible to do so without your guidance.

I would like to express my heartiest gratitude to my supervisor Prof. Dr. Joachim Heberle for his guidance and encouragement in my interest in this field and for giving me the opportunity to work on this interesting topic.

I sincerely thank my supervisor Priv.-Doz. Dr. Michael Haumann for the discussion of my work as well as reviewing my thesis.

Furthermore, I want to thank Alexei Sirbu for guiding and advising me during my work. I very much appreciate your patience and our discussions.

I would like to acknowledge the help and support from the members of Receptor Signaling Lab (Max-Delbrück-Centrum für Molekulare Medizin). Thanks for the fun chat time in the office and for helping me in dealing with the instruments whenever I was stuck.

Last but not least, I am thankful to my family for all the support during my studies abroad, especially to my parents, without their support I would not have achieved it. I also want to thank my friends for motivating me during my work and for answering my questions and clarifying my doubts whenever I approached them.

This thesis is dedicated to my parents.

Contents

List of Tables

List of Figures

Chapter 1

Introduction

Since the observation of fluorescence properties of quinine by Sir John Frederick William Herschel in 1845 [Herschel, 1845], fluorescence has become a vital tool for the observation of the structure of cells and tissues. The development of fluorescent spectroscopy and microscopic techniques has made a significant contribution to solving several problems of biological systems [Engelborghs and Visser, 2014]. While X-ray crystallography and electron microscopy can achieve atomic resolution, these approaches cannot be employed on living samples, as they work on the imaging in a non-native environment at cryogenic temperature. By using advanced fluorescence microscopy techniques, the image of the biological samples can be obtained in the living environment with high resolution. Current advances in super-resolution microscopy and high-resolution fluorescence spectroscopy techniques yield the necessary temporal and spatial resolution to image fluorescently labelled molecules in their native environment [Lakowicz, 2006a].

Steady-state and time-resolved fluorescent spectroscopies can be used to study the molecular properties of fluorescent dyes, such as chemical composition, lifetime and anisotropy, etc. This report presents the basic concepts of fluorescent spectroscopy and microscopic techniques, together with the experimental setup and the application of these concepts to characterise real-life molecules that were the target of our study.

1.1 Motivation

The Receptor Signaling group has recently published research characterizing a fluorescent cAMP-analogue's uptake and subcellular distribution, based upon conjugating cAMP to fluorescein diacetate (FDA). This molecule was named 8-FDA-cAMP [Bock et al., 2020]. FDA is cell membrane permeable esterase substrate, which upon de-esterification, yields the well known and characterized fluorophore fluorescein. In the context of a blind drug screening assay, we received two fluorescent drug analogues from external collaborators based on the conjugation of two drugs expected to bind intracellular proteins to FDA. The two compounds are indicated as MAN193 and AG3457 . My project aims to characterize those drug analogues in terms of fluorescent properties and cellular uptake, together with the previously employed 8-FDA-cAMP. The goal of my master thesis is achieved by employing fluorescence spectroscopy, lifetime and anisotropy in the cuvette, as well as confocal microscopy to characterize the cellular uptake of the three compounds.

Chapter 2

Basic principles of fluorescence spectroscopy

2.1 Principle of fluorescence

The fundamental principle of fluorescence was first reported by Sir John Frederick William Herschel in 1845 [Herschel, 1845]. He observed the faint blue light emission from the quinine in tonic water upon excitation with the ultraviolet component of sunlight. The process of light generation from a substance through energy conversion is known as luminescence. The fundamental mechanism of fluorescence can be well explained by the $Jablonski\ diagram$ shown in Figure 2.1.

The process of absorption and subsequent re-emission of light from the molecules can be well understood by the Jablonski diagram. From the diagram (2.1), S_0 stands for the singlet ground state and S_1, S_2 are the singlet excited states, respectively. Each electronically excited state consists of different vibrational energy levels 0,1,2,3 etc. When a photon of a specific wavelength is incident on the molecule, then the absorption takes place. Due to absorption, a vertical transition takes place from the ground state to the excited singlet state ($S_0 \rightarrow S_2$) in a period of less than a few femtoseconds. The molecule relaxes back to the lowest excited vibrational level by the process of internal conversion, which occurs in order of picoseconds. Finally, the molecule relaxes to the ground state by emission of fluorescence and the lifetime of a fluorophore is typically in the order of a few nanoseconds. The absorption and fluorescence of a molecule takes place from the lowest vibrational energy levels. The molecules which

is in the S_1 singlet excited state, can undergo a spin a spin transition to the T_1 triplet excited state by Intersystem crossing. The emission of light from the triplet excited state T_1 is known as the phosphorescence. The lifetime of phosphorescence can range from a few microseconds to a few seconds [Valeur, 2001].

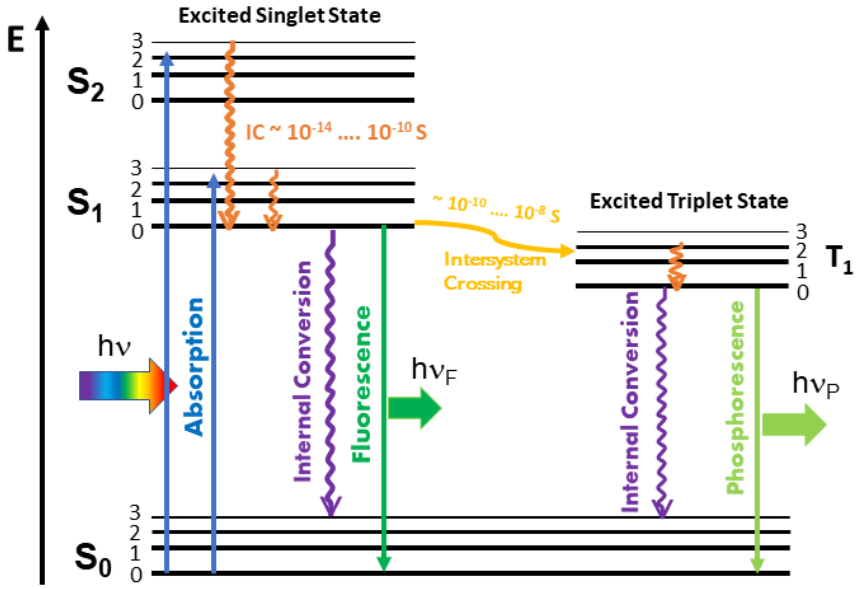

Figure 2.1: Jablonski diagram: S_0 is the singlet ground state and S_1, S_2 are the singlet excited states . The excitation and de-excitation pathways are shown in the system with corresponding time scale, the transition pathways from S_2 to S_1 is known as the internal conversion (IC). On the right hand side of the diagram T_2 represents the excited triplet state and the transition from S_1 to T_1 is known as the Inter-System Crossing (ISC).

During the internal conversion, there is a loss in energy occurring due to the vibration of the molecules, which results in the shift in the emission spectrum, known as the Stokes shift observed by Sir. G. G. Stokes in 1852 shown in Figure 2.2. The energy carried out by photons is inversely proportional to their wavelength ($E = h\nu$). Due to the vibrational loss of energy of the molecule in the excited state the energy of emission after coming back to the ground state decreased. As the energy of the photon is directly proportional to its wavelength, a red shift of the fluorescence spectrum can be observed (Figure 2.2). The emission and excitation spectra of a fluorophore can be obtained by using the steady-state spectrofluorometer. The quantum yield and the emission spectra of most fluorophores are independent of the excitation wavelength. Hence the absorption spectra are superimposed with the excitation spectrum [Lakowicz, 2006c].

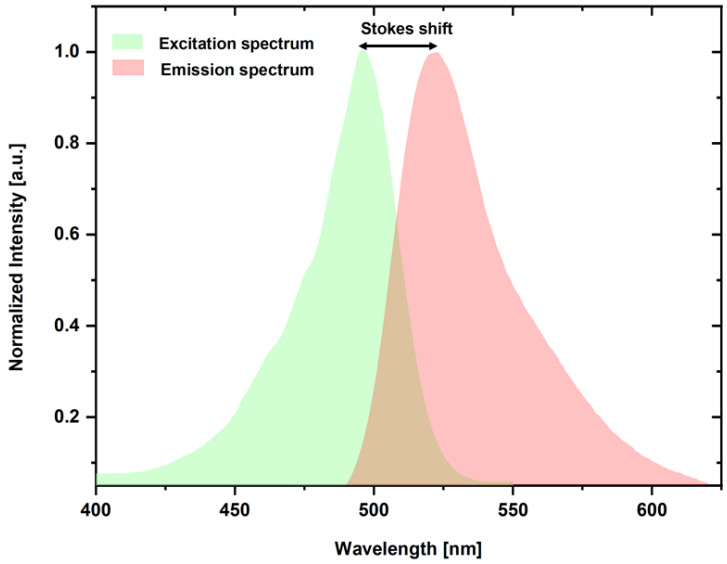

Figure 2.2: Stokes Shift: A typical diagram to explain the stokes shift for a fluorescent dye MAN194 was used for this thesis. This diagram shows the excitation and emission spectrum of MAN194 at 5-nm band-pass obtained by exciting the light of 450 nm and scanning the emission 1 nm steps with 1-s integration from 470 to 650 nm. The excitation and emission spectrum of MAN194 are represented by the green and red shaded area respectively

2.1.1 Fluorescence lifetime and quantum yields

The fluorescent lifetime and quantum yield are two essential, and interconnected properties of fluorophores. The fluorescence lifetime indicates the average time spent by the molecule in the excited state before coming back to the ground state. Typically fluorescence lifetimes are in the order of a few nanoseconds. From the $Jablonski\ Diagram$ we know the relaxation of the fluorophore to the ground state 'S_1' takes place in two different ways. One is the emissive rate of the fluorophore 'Γ', which corresponds to the fluorescence emission, and the other is non-radiative relaxation 'K_{nr}' without any fluorescence emission.

The lifetime that a fluorophore spends in the excited state is thus given by the formula

$$\tau = \frac{1}{\Gamma + K_{nr}} \tag{2.1}$$

In the absence of a non-radiative process, the lifetime of fluorophores is called an intrinsic or natural lifetime. The decrease in the non-radiative process increases the fluorescent lifetime, which results in a brighter emission from a fluorescent molecule. The natural lifetime of a fluorophore is expressed by

$$\tau = \frac{1}{\Gamma} \tag{2.2}$$

The quantum yield is defined as the ratio of the number of photons emitted to the number of photons absorbed. In the previous section, the emission of fluorescence due to the de-excitation of fluorophores to the ground state was discussed. However, part of the energy is not emitted in the form of light during the depopulation to the ground state, and this is known as non-radiative relaxation. The quantum yield for a fluorophore is expressed by

$$Y = \frac{\Gamma}{\Gamma + K_{nr}} \tag{2.3}$$

The quantum yield (Y) can approach unity when the nonradiative decay rate is significantly lower than the radiative decay rate $K_{(nr)} << \Gamma$.

2.2 Absorption spectroscopy

The measurement of absorbance is one of the basic techniques of fluorescent spectroscopy, as it calculates the amount of the intensity of light lost during the absorption process in a medium. The amount of light absorbed by the molecule upon excitation by a particular wavelength of light is known as absorbance. Similarly, the intensity of light transmitted with respect to the intensity of incident light is known as transmittance. The principle of measurement of absorbance is formalized by the Beer-Lambert law [Valeur, 2001].

The quantification of absorbance of the molecules studied in this work was done by using a UV-Vis spectrophotometer. UV-Vis spectroscopy is a quantitative technique used to determine the proportion of light absorbed by the chemical substance. This experimental techniques was used to study the absorbance properties of the novel fluorescent drug analogues dissolved in a buffer. Figure 2.3 displays the experimental layout of a UV-Vis spectrophotometer, where the Xenon lamp is used as a light source due to its broad-spectral ranges from (200-750) nm. The excitation light passes through a monochromator selecting the particular wavelength for excitation. After passing through the monochromator, excitation light is split into two different pathways. The light rays collimated through the reflector

lenses excites the fluorescent sample placed in a quartz cuvette (solution) and a solvent placed in a quartz cuvette in front of the reference beam. There are two detectors used to measure the signal, one is for the sample(solution) and another one is for the reference (solvent) beam.

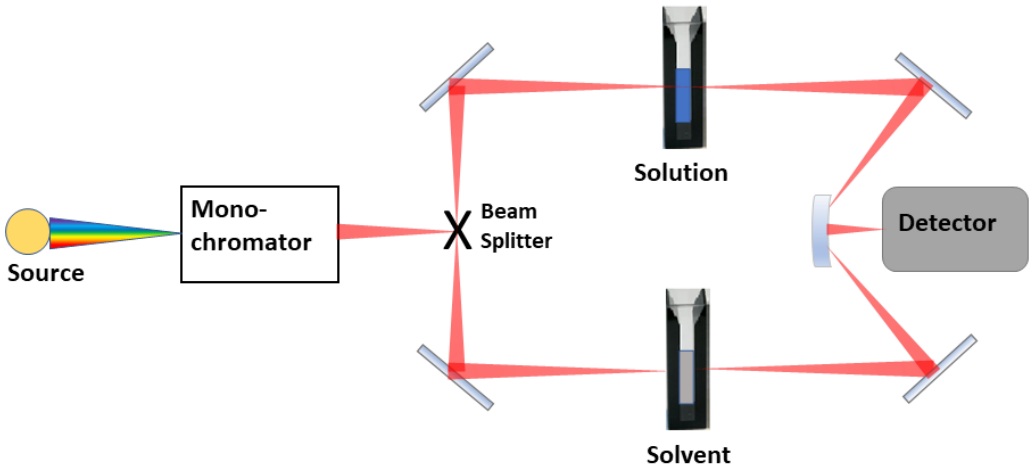

Figure 2.3: Typical diagram for the UV-Vis spectrometer experimental setup.

The UV-Vis spectrophotometer uses two beam paths for the measurement purpose, the first to measure the absorbance of the solution and the second (through the solvent) to measure the background. The measurement of background is due to the presence of optical scattering of the solvent present in the fluorescent solution. The noise of the absorption spectrum can be obtained by measuring the background of the solvent from the reference beam. Finally, the data obtained from the fluorescent solution to the background is subtracted to get the final results for absorbance. When a fluorescent sample interacts with the collimated excitation light absorption takes place, several molecules within the solution go to the excited state, emitting isotropically light at a higher wavelength (due to the Stokes shift). The amount of light at the original excitation wavelength that comes out of the sample is therefore reduced due to this absorption process [Valeur, 2001]. Each molecule is associated with a photon capture area, known as absorption cross-section σ. The probability of photon absorption depends both on that cross-section and the concentration of the molecules in the cuvette. This number is given by the formula:

$$log\left(\frac{I_0}{I}\right) = N_a \cdot \sigma \cdot c \cdot l \, \frac{1}{2.303} \tag{2.4}$$

Where, N_a stands for the Avogadro's number, σ represents the absorption cross-section of the molecule,

c is for the molar concentration of the solution and l is the optical path length of light travelled through the cuvette.

The absorption of the number of photons passing through a solution is well defined with the help of Beer-Lambert Law [Valeur, 2001]. Each molecule has an absorption cross-section that depends on the wavelength; hence the absorbance of a molecule by Beer-Lambert law is given by

$$A(\lambda) = log\frac{I_\lambda^0}{I_\lambda} = \varepsilon(\lambda)\, lc \tag{2.5}$$

Where ε represents the molar extinction coefficient, that can be written as

$$\varepsilon(\lambda) = \frac{N_a}{2.303}\,\sigma$$

2.3 Steady-state fluorescenece spectroscopy

In steady-state fluorescence spectroscopy, the intensity and spectral profile of fluorescence emission can be observed with a continuous illumination using an excitation beam. As discussed in the previous section, the typical fluorescent lifetime of fluorophores lasts from hundreds of picoseconds to tens of nanoseconds. When a fluorescent sample is exposed to light, steady-state is achieved almost immediately. The steady-state experimental setup deals with an advanced photodetection system and superior signal to noise ratio . Hence most of the molecular information can easily be obtained in steady-state measurements. The steady-state experiment is used to get faster information such as spectra, lifetime or anisotropy of the fluorescent samples investigated. [Lakowicz, 2006a].

In the case of the steady-state fluorescence, the output result is the time-average of the data of each time point.

The steady-state intensity related to the decay time is stated by the relation

$$I_{steady-state} = \int_0^\infty I_0\, e^{-\frac{t}{\tau}}\, dt = I_0\tau \tag{2.6}$$

The value of I_0 depends on the fluorophores concentration and instrumental parameters.

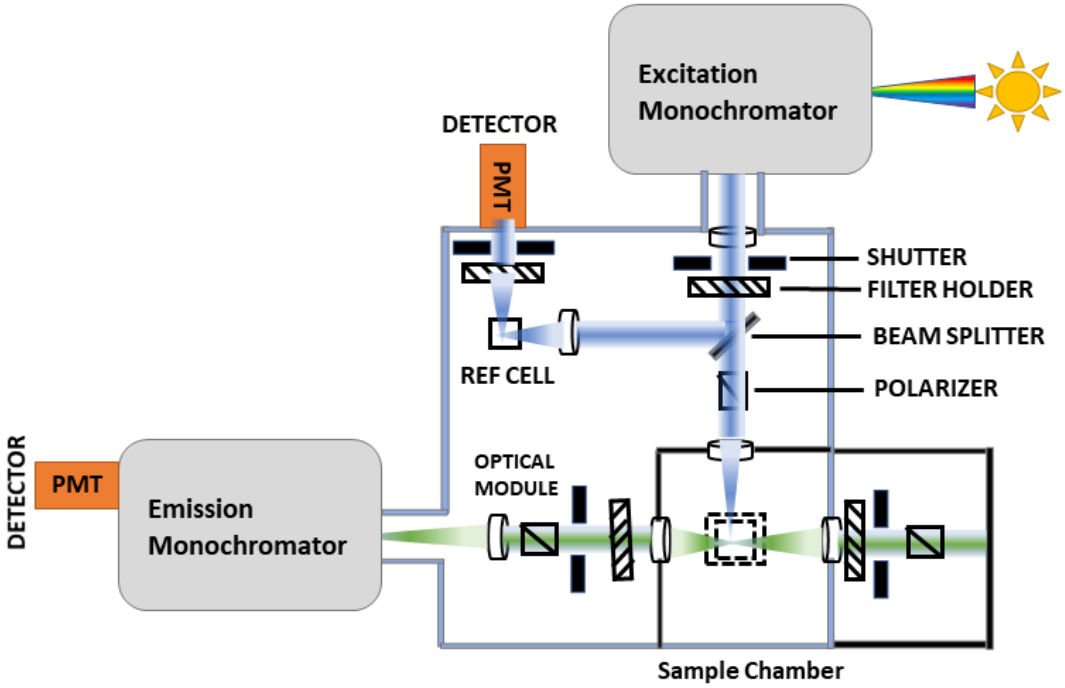

Figure 2.4: Schematic diagram for the steady-state sectrofluorometer experimental setup. The excitation source is a Xenon lamp and two photomultiplier tube detectors are used for detection.

From Figure 2.4, we can see a typical diagram for a steady-state spectrofluorometer experimental setup, where the excitation source is a Xenon lamp due to its high intensity and the broad range of wavelength selection available for excitation. The light rays then pass through an excitation monochromator to select a particular wavelength of excitation. After passing through the monochromator, the light ray passes through a series of optical modules and interacts with a beam splitter. The beam splitter reflects a part of the light to a reference cell. The beam splitter is made of pure quartz crystal, and it reflects only 4% of the incident light. Then the light passes through a polarizer to the sample chamber. The excitation light interacts with the fluorescent sample in a quartz cuvette inside the sample chamber, and the emission light passes through the same series of optical modules to the emission monochromator. The emission ray passes through the emission monochromator and reaches the detector. The polarizer is also present in the emission path. It is useful in the case of the measurement for fluorescence anisotropy.

The spectrofluorometer is widely used because its high signal-to-noise ratio and high-sensitive photomultiplier tube detector. Figure 2.5 represents the schematic diagram of the photomultiplier tube (PMT) detector used in the spectrofluorometer. From the Figure 2.5, it can be seen that the dynodes are held together at a negative potential. When a photon hits the photocathode, an electron is emitted. The

potential difference between the photocathode and anode accelerates the electron; as a result, it moves with high speed and it interacts with the other dynodes resulting in more electrons. After several transitions with several dynodes, multiple electrons finally arrive at the anode and output signal intensity increases. When a photon with low intensity arrives at the detector, a high-intensity signal obtained in the output due to the electron multiplication by the photomultiplier tube inside the detector.

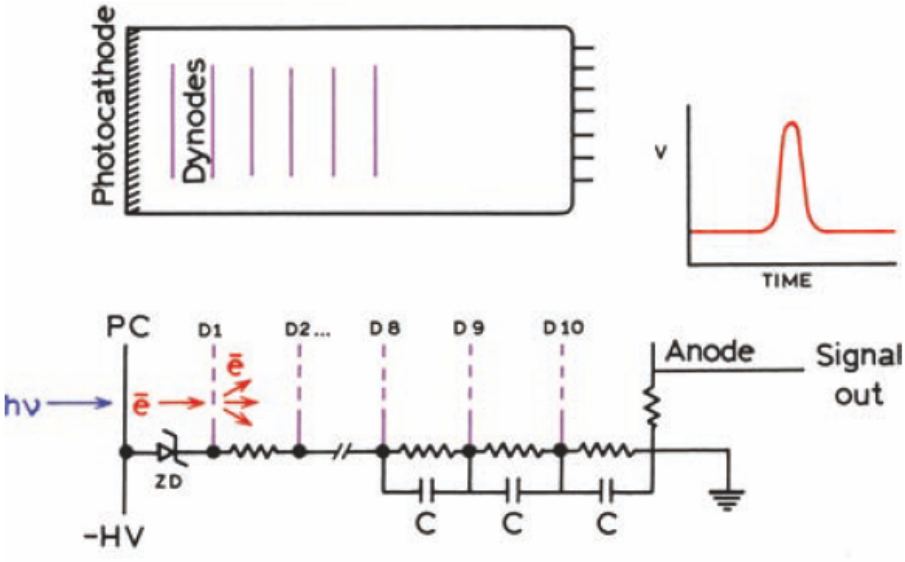

Figure 2.5: Schematic diagram of a photomultiplier tube and its dynode chain [Lakowicz, 2006c].

2.4 Time-resolved fluorescence spectroscopy

In steady-state experiment we work with the averaging process, and the lifetime of the excited state of the fluorescent sample is lost during the averaging process [Lakowicz, 2006d]. Time-resolved spectroscopy is used to measure the dynamic process of the fluorescent compounds in the picosecond time domain. In the case of time-resolved fluorescent spectroscopy, a femtosecond pulsed laser diode is an excitation source. By the use of time-resolved fluorescent spectroscopy, the lifetime and time-resolved anisotropy of a fluorescent sample can be easily obtained. If more than one fluorescent species are mixed, observing the information using the steady-state spectrofluorometer is inadequate due to spectral overlap. By using a time-resolved fluorescence spectroscopy experiment, the different fluorescent lifetimes of more than one fluorescent sample with overlapping emission spectra can be observed [Laine, 2013].

Let us say a fluorescent sample is excited by using a pulsed laser source, and n(t) is the population of fluorophores that goes to the excited state. The decay of excited state population with time is given by

$$\frac{dn(t)}{dt} = -\left(\Gamma + K_{nr}\right)\ n(t) \tag{2.7}$$

Where n(t) is the number of molecules in the excited state, Γ refers to the emissive rate of the molecule and K_{nr} is the non-radiative decay, as we have seen previously. As the emission is a random event and each fluorophore has a constant probability of emission within a certain time period, the solution to the differential equation above is an exponential decay:

$$n(t) = n_0\ e^{\frac{-t}{\tau}} \tag{2.8}$$

Where τ stands for the lifetime of the fluorescent molecule. he lifetime τ is the inverse of the decay rate [Lakowicz, 2006d] $\tau = (\Gamma + K_{nr})^{-1}$. The time dependent intensity $I(t)$ related to the lifetime of the fluorescent sample can be written as

$$I = I_0\ e^{\frac{-t}{\tau}} \tag{2.9}$$

Where I_0 is the intensity at time zero.

2.5 Time correlated single photon counting (TCSPC)

Time correlated single photon counting (TCSPC) is a well known approach for determining fluorescence lifetime [Horiba, 2009]. The diagram in Figure 2.6 represents the typical setup for time-correlated single-photon counting (TCSPC). A 405 nm pulsed laser diode (Delta diode) is used as an excitation source and is connected by a diode laser driver to the timing electronics as shown in Figure 2.6. The light pulse passes through a polarizer and is then collimated through a lens to the sample chamber. The light pulse then reaches the sample chamber, where we kept the fluorescent sample in a quartz cuvette. The emission light passes through a long-pass filter to the detector. We used an advanced hybrid

picosecond photon detector (HPPD) for photon counting in TCSPC instrumentation, which combines the benefits of conventional PMT designs (wide spectral response and large active area) to achieve good detection efficiency. A detector controller controls the switching of the detector, and the detector controller is connected to the timing electronics as shown in Figure 2.6.

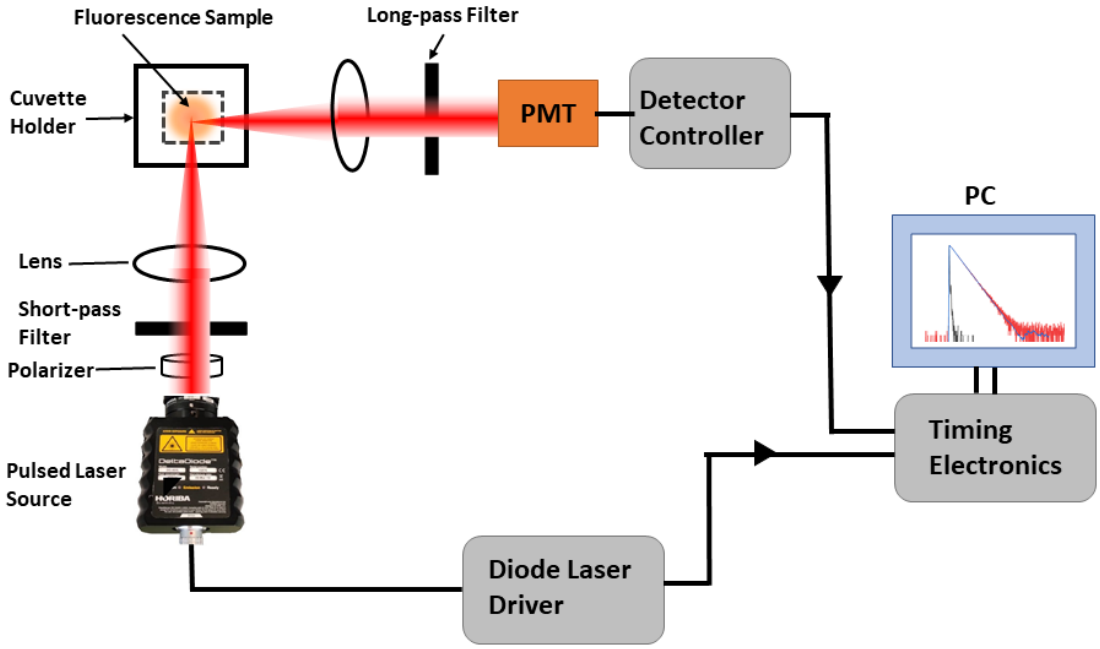

Figure 2.6: A typical experimental setup for fluorescence decay measurement with TCSPC.

Time correlated single photon counting (TCSPC) works with the advanced detection system to record the low energy photons. The TCSPC instrumentation is based on the single-photon counting system with periodic laser pulses. The difference between the excitation and emission time is measured by the detector electronics, which acts as a stopwatch [Wahl and Orthaus-Müller, 2014]. The detector starts photon-counting after excitation of each laser pulse and stops counting when the fluorescent photon reaches the detector. The number of photons counted by the detector for single excitation should be either one or zero, and this value is reflected by the experimental parameter α during the measurement. The experimental parameter α depends on the number of photons arriving at the detector per unit time, and ultimately depends upon the excitation light intensity and the fluorescent sample's concentration. According to the single photon probability condition, there would not be any photon from many cycles after the laser pulse, as shown in the second cycle of Figure 2.7. For each excitation pulse, the detector counts the arrival of each photon for a certain time and arrange them on a time axis. After counting thousands of photons and placing them on a histogram with the time axis shown in the Figure 2.7(b),

we fit an exponential decay function with the histogram of data to obtain fluorescent decay's lifetime and nature of the decay curve.

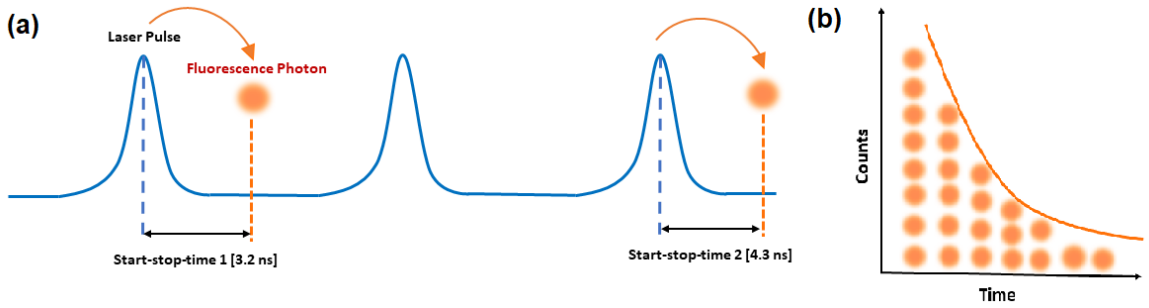

Figure 2.7: (a) Measurement of start and stop time in time-resolved fluorescence with TCSPC, (b) Histogram of photon arrangement with respect to the arrival time in TCSPC measurement.

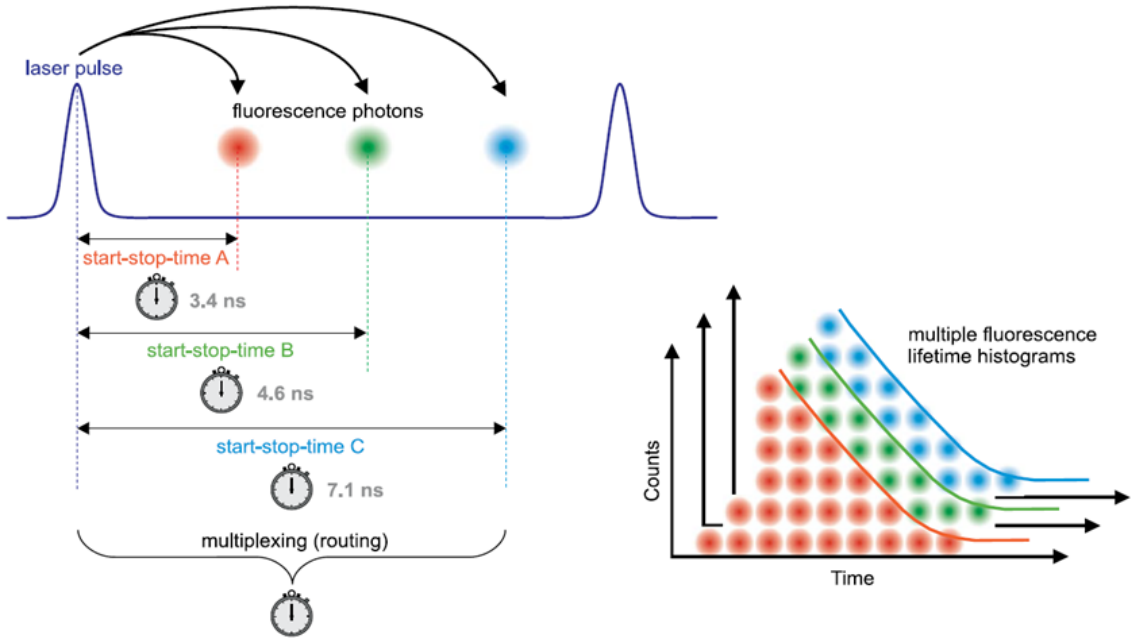

Figure 2.8: Multichannel TCSPC with multiple fluorescence lifetime histograms [Wahl, 2014]

In some cases, more than one photon is possible during the excitation, and this term is known as the "photon pile-up". For each excitation, the detector counts the single photons and if more than one photon arrives, the detector measures the first one, and the rest are not counted, since the detector goes into a hibernation state and stops counting photons up to the next excitation pulse, known as the detector's dead-time. Although the detector only counts the photon that arrives first, the increase in fluorescent photons affects the decay pattern and changes the lifetime. Hence, for the TCSPC experiment, the experimental parameter "α" is maintained by the system to less than 2% to avoid the photon

pile-up. For multi-exponential decays, in order to obtain the fluorescent lifetime and decay curve, the histogram of the data is fitted with more than one exponential fit as shown in Figure 2.8.

2.6 Fluorescence anisotropy

Fluorescence anisotropy (directly related to fluorescence polarisation) is the measurement of the change in orientation of molecules in space corresponding to the time between absorption and emission. The principle of anisotropy deals with the transition dipole moment of absorption and emission that lies along with the specific orientation of the fluorophore structure.

For the measurement of anisotropy we used the steady-state and time-resolved spectrofluorometer setup (Section 2.3) with polarized emission and excitation light. The steady-state and time-resolved polarization excitation and emission spectra were obtained on a spectrofluorometer using a 10 mm side quartz cuvette, holding a volume of up to 600 µL of solution. In the case of steady-state measurements, the Xenon lamp was used as an excitation source; in the case of time-resolved measurements, the pulsed laser source described above was used as the excitation source. Four polarized intensity measurements were taken per experiment using two polarizers. One is located in front of the excitation source to get the polarized excitation, and the second one is located between the sample and detector to obtain the polarized emission. The four polarization measurements, corresponding to the possible combinations of polarizers orientations are: $I_{VV}(\lambda)$, $I_{VH}(\lambda)$, $I_{HH}(\lambda)$ and $I_{HV}(\lambda)$. The subscript V, H refers to the horizontal and vertical polarized excitation and emission. The schematic diagram for the principle of anisotropy is explained in Figure 2.9, where we used the light source of vertical excitation and measured the polarized excitation and emission intensities by the detector.

The method of fluorescence anisotropy is widely used in life sciences for the quantification of protein-protein interaction in micro and nanomolar concentration range [Valeur, 2001]. The fraction of free and bound ligand during the protein-ligand interaction can be obtained by using fluorescence anisotropy, which monitors the intensity of polarization for parallel and perpendicular light. When the emission polarizer is oriented parallel to the direction of polarized excitation, the observed intensity is called I_{VV}. Similarly, when the polarizer is perpendicular to the excitation, the observed intensity is called

I_{VH}. Hence, the formula for the anisotropy is given by the equation,

$$r = \frac{I_{VV} - GI_{VH}}{I_{VV} + 2GI_{VH}} \tag{2.10}$$

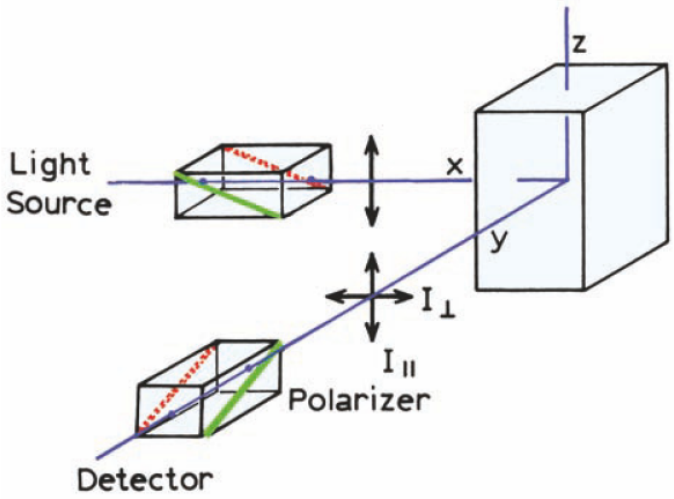

Figure 2.9: Schematic diagram for the working principle and measurement of fluorescent anisotropies [Lakowicz, 2006b]

Where the term G is known as the instrument "G-factor" corresponds to the efficiency ratio between the detection paths [Teijeiro-Gonzalez et al., 2020]. The G factor is the instrument sensitivity ratio towards the vertically and horizontally polarized light. The G-factor of the instrument is given by the relation

$$G = \frac{I_{HV}}{I_{HH}}$$

In time-resolved fluorescence anisotropy, the sample is excited by vertically polarised light pulses; simultaneously, the intensity decay of the specimen is measured by a polarizer oriented vertically and horizontally to the sample. The time-resolved anisotropy r(t) is given by

$$r(t) = \frac{I_{polarized}(t)}{I_{total}(t)} = \frac{I_{VV}(t) - GI_{VH}(t)}{I_{VV}(t) + 2GI_{VH}(t)} \tag{2.11}$$

Where G is known as the instrumental sensitivity ratio, corresponds to the efficiency ration between the detection paths.

In fluorescence anisotropy, a sample's polarisation states are obtained by illumination with vertically polarized light. If the absorption dipole of fluorophores coincides with the vertical excitation, then the fluorophores are preferentially excited, and this process is known as the excitation photo selection. An analyzer measures the emission from the fluorophore at a polarization angle θ with respect to the angle of excitation polarization [Lakowicz, 2006b]. The intensity of fluorescence measured at a polarization angle θ is given by

$$r_0 = \frac{2}{5}\left(\frac{3cos^2\theta - 1}{2}\right) \tag{2.12}$$

For the measurement of time-resolved anisotropy, a pulsed laser is used as an excitation source. The time-resolved decay curve can be obtained by exciting the fluorescence sample with the laser, and the decay curve is then fitted with the following equation to obtain the rotational correlation time and anisotropy of the molecule.

$$R_t = R_\infty + (R_0 - R_\infty)\, e^{-\frac{t}{\tau}} \tag{2.13}$$

Where R_0 is anisotropy of the sample when $t = 0$, and R_∞ is anisotropy of the sample when $t = \infty$. The rotational correlation time of the fluorescent sample is given by τ.

The rotational correlation time for the molecule can be expressed by the equation,

$$\theta_{rot} = \frac{\eta V}{K_B T}$$

Where, V is the molecular volume, T stands for the temperature and K_B is the Boltzmann constant. The term η represents the microviscosity of the molecule within the cuvette. The microviscosity η of a molecule depends on its molecular weight and increases with the increase of molecular weight at constant composition.

2.7 Confocal microscopy

Confocal microscopy is a widely used imaging technique, that was first proposed in 1957 by the American mathematician Marvin Minsky. He used the combination of a lamp, a pinhole, lenses, and a detection system to image the living cells by illuminating the light on the sample. However, due to technical limitations at the time, Minsky was unable to achieve a good resolution. Also, the microscope was limited by the technology at that time with low scanning speed photodetection. Now, the advancement of high spatial resolution confocal microscopy allows investigating the different proteins in living cells with high resolution. With the development of spatially resolved fluorescence microscopy system, we can visualize the subcellular compartment of living cells with adequate resolution [Murphy and Davidson, 2012].

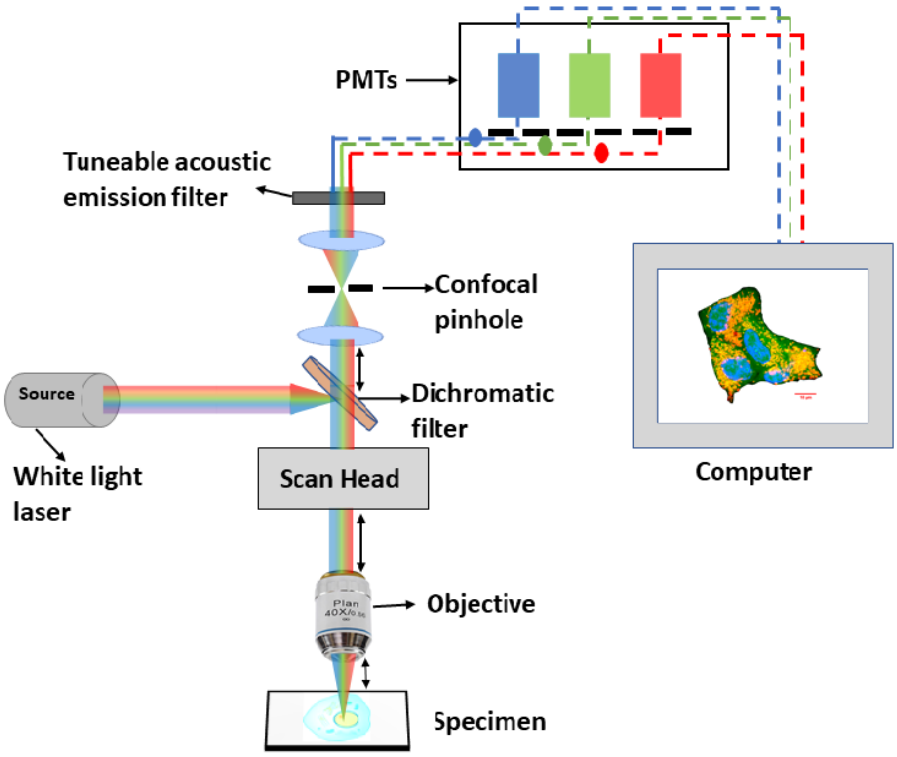

Figure 2.10: Schematic diagram for the laser scanning confocal microscope setup.

Figure 2.10, illustrates the schematic diagram of a confocal microscope. The laser is the excitation source and is reflected towards the objective by using a dichroic mirror. The scan head contains mirrors that tilt the angle of the beam hitting the back focal plane of the microscope objective, thus allowing linear scanning of the collimated excitation spot (known as microscope excitation volume) within the imaging

plane. The fluorescence light emitted from the specimen is collected by the objective, goes back through the scan head, and reaches the confocal pinhole, which selects only in-focus light. The light passing through the confocal pinhole is then wavelength selected through a tunable acoustic emission filter, which splits the individual wavelengths of light. The different wavelengths of light passing through the filter are then focused through lenses to the photodetector. Our experimental setup was a Leica SP8 microscope, based on a white light laser source and hybrid (HyD) photodetectors.

The lateral resolution of the confocal microscope depends on the focusing of the laser light by an objective. The resolution limit of the microscope at a particular wavelength λ is defined by the so-called diffraction limit d:

$$d_{lat} = 0.61 \, \frac{\lambda}{NA} \tag{2.14}$$

Where NA is known as the numerical aperture of the objective ($NA = \ n \cdot SIN(\alpha)$), represents the angle up to which the amount of light collected by the objective. Here n stands for the refractive index of the medium, and the maximum collective angle of light by the objective is given by α.

As the confocal pinhole is placed in a conjugate optical plane with respect to the the sample plane, the purpose of using the confocal pinhole is to reject the light coming from the out of focus emission from the objective plane. Hence, the confocal microscope's axial resolution depends on the confocal pinhole's ability to reject the out of focus light coming from the emission. The formula for the axial resolution of the confocal microscopy is given by

$$d_{ax} = \ \frac{2n\lambda_0}{NA^2} \tag{2.15}$$

Where n is the refractive index and λ_0 is the wavelength of light emitted from the sample.

2.8 Fluorescein diacetate as a cell permeable label

Fluorescein belongs to a family of versatile, functional dyes, which have been widely used due to its excellent fluorescence and superior photophysical properties [Zhang et al., 2014]. The acid-base equi-

librium state of fluorescein dye depends on the solvent in which it dissolved, which changes its chemical structure and results in different fluorescence properties. The fluorescein diacetate (FDA) compound is prepared from the FDA powder, which is in a dark state. When the FDA power is dissolved in a buffer of pH > 9, with 1 M NaOH at 50 degree temperature for more than 24 hours, then FDA turns into fluorescein due to the hydrolysis at higher pH as shown in Figure 2.11.

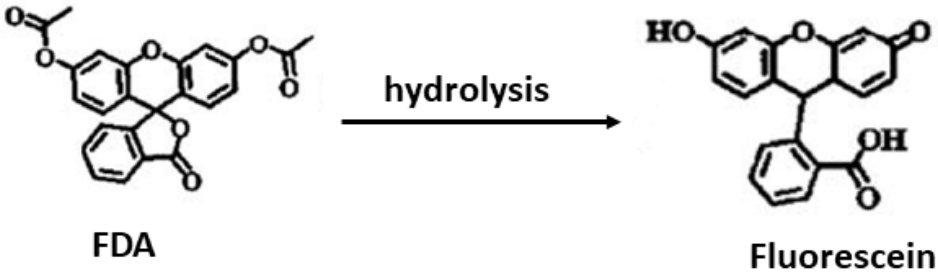

Figure 2.11: The molecular diagram for the conversion of FDA into fluorescein by hydrolysis.: The molecular structure represents the conversion of fluorescein diacetate into fluorescein due to the hydrolysis at higher pH, which results in the activation of the compound from the dark state to fluorescence [Zhong, 2009].

Fluorescein is the most commonly used fluorescent probe due to the availability of a wide range of excitation wavelength selections. Its very high molar absorptivity at a wavelength range of 488 nm, large quantum yield, and high photostability makes it beneficial for high sensitive fluorescent experiments [Sjöback et al., 1995]. Fluorescein diacetate (FDA) is also widely used for microscopy experiments due to its brightness and higher quantum yield. FDA is a cell-permeable label and when it enters into the cell becomes fluorescein due to the intracellular esterases.

2.9 8-FDA-cAMP a cell-permeable fluorogenic cAMP analogue

Cyclic adenosine monophosphate (cAMP) is a second messenger synthesized by adenylyl cyclase within the G protein-coupled receptors (GPCRs) signaling pathway. The understanding of the dynamics of cAMP in the intercellular environment was aided by the development of 8-FDA-cAMP fluorescent analogue ([Bock et al., 2020]). The structure for the 8-FDA-cAMP fluorescent analogue is represents in the Figure 2.12. The 8-FDA-cAMP is cell-permeable analogue and becomes fluorescent (8-F-cAMP) when hydrolysis of the two ester bonds per molecule in the intercellular environment occurs by cellular es-

terases. The 8-F-cAMP molecule (the de-esterified 8-FDA-cAMP analogue) is a widely used fluorescent probe to understand the activation of downstream signaling in GPCRs.

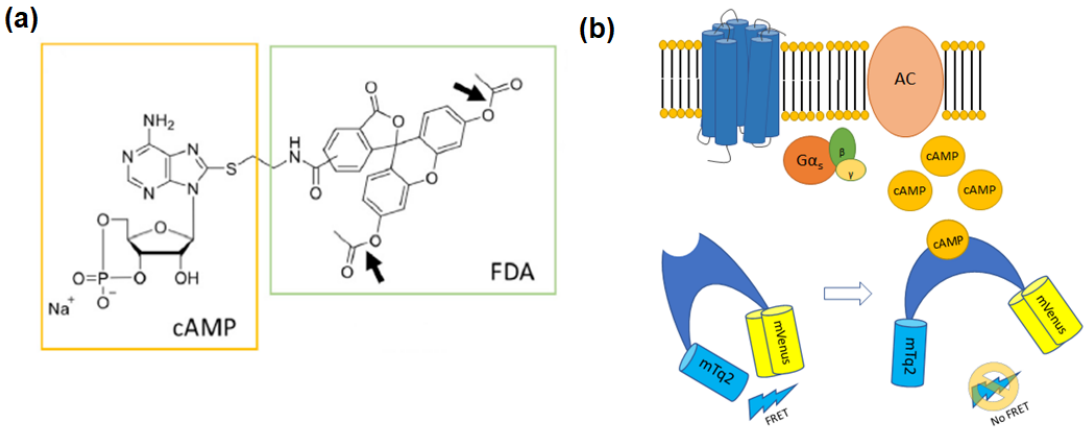

Figure 2.12: (a) The molecular structure of 8-FDA-cAMP molecule, highlighting the location of ester bonds. (b) This diagram represents the cAMP production downstream of a G protein-coupled receptor (GPCR) activation [Bock et al., 2020].

Chapter 3

Spectroscopic characterization of novel fluorescent drug analogues

3.1 Measurement of absorbance

Measurement of absorbance is a quantitative technique used to evaluate the amount of light absorbed by a chemical substance. This can be translated into a precise concentration measurement, or, to estimate the molar extinction coefficient (EC) of compounds of known concentration. The characterization of a novel fluorescent drug analogue largely relies on the measurement of absorbance. Here we investigated the absorption properties of the novel fluorescent drug analogues by employing absorption spectroscopy. The Evolution 350 UV-Vis Spectrophotometer (ThermoFisher Scientific) was employed for this experiment. For measurement, a quartz cuvette (Hellma Analytics) of path length 10 mm was used within the UV-VIS spectrophotometer. The results for the absorbance was obtained after optimizing the noise reduction from the experimental data by increasing the integration time of the spectrometer. A nominal concentration of 1 μM of each drug analogue, prepared from powder, was used for measuring the absorbance based on their optimal spectral behaviour. The initial stock concentration of the molecule was 100 μM, then diluted it in the TRIS buffer of pH 8 in a 1:100 dilution for the final measurement. The absorbance for activated and non-activated states of fluorescein, 8-F-cAMP, MAN194 and AG3457-activated molecules were represented in Table 3.1. For being activated AG3457 molecule was diluted in TRIS buffer of pH 9 with 24 h of incubation at 50 $^{\circ}C$.

Fluorescein was employed as a reference for this experiment to compare the results obtained from absorption spectroscopy. At first, absorbance of the solvent was obtained in TRIS buffer and then we obtained the absorbance of the molecule after subtracting background data.

Molecule in activated state	Molecule in non-activated state
Fluorescein	Fluorescein diacetate
8-F-cAMP	8-FDA-cAMP
MAN194	MAN193
AG3457-activated	AG3457

Table 3.1: This table shows the naming convention for the molecules in activated (fluorescein) and non-activated (FDA) fluorescent state.

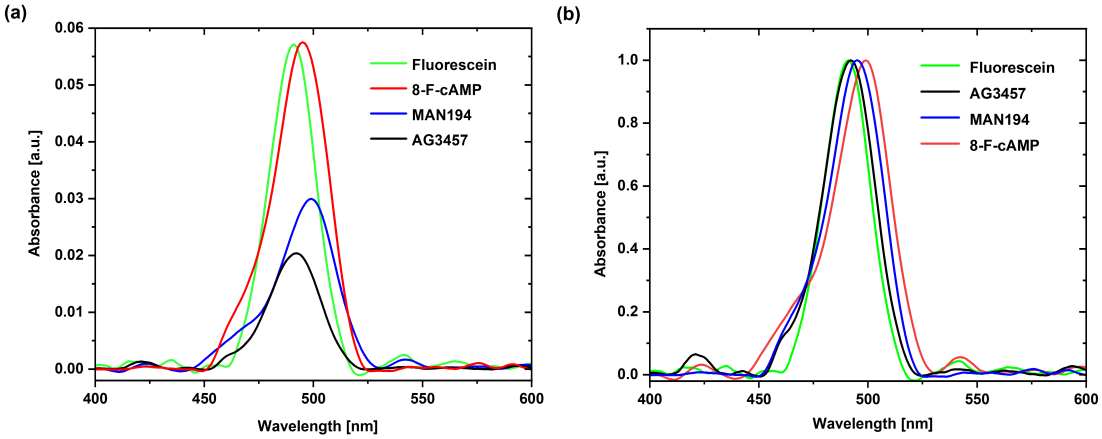

Figure 3.1: Absorbance of fluorescent analogues: (a) Absorption spectra of fluorescent analogues, where absorbance of each molecule shown with respect to the wavelength ($\lambda_{ex} = 470\,nm$). (b) The absorption peak of the fluorescent molecules corresponding to the particular wavelength obtained after subtracting the background noise.

The absorbance of fluorescein and 8-F-cAMP was roughly double that of MAN194 (Figure 3.1); however, the absorbance of AG3457-activated was less than that of MAN194 (Figure 3.1). For this experiment, the fluorescein molecule was used as a control. Moreover, 8-F-cAMP has a somewhat higher absorbance than fluorescein. The absorbance of fluorescent analogues was used to calculate the extinction coefficient for each luminous molecule. Fluorescein exhibited an extinction coefficient of $\epsilon = 58000\ M^{-1}cm^{-1}$, while 8-F-cAMP, MAN194, AG3457-activated has an extinction coefficients of $\epsilon = 59000\ M^{-1}cm^{-1}$, $\epsilon = 29000\ M^{-1}cm^{-1}$ and $\epsilon = 18000\ M^{-1}cm^{-1}$. The extinction coefficient of pharmaceutical analogues were summarized in Table 3.2. The probability of photon absorption by fluorescein and 8-F-cAMP is exceptionally high when compared to MAN194 and AG3457-activated. The

peak for the absorbance of each fluorophore was computed using absorbance normalization, as shown in Figure 3.1. Fluorescein and AG3457-activated absorbance maxima were identical; however, the absorption peak for MAN194 and 8-F-cAMP was red-shifted by approx. 10 nm and 20 nm, respectively.

Molecule	Absorbance	Extinction coefficient ($M^{-1}cm^{-1}$)
Fluorescein	0.058	58000
8-F-cAMP	0.059	59000
MAN194	0.029	29000
AG3457-activated	0.018	18000

Table 3.2: Calculated extinction coefficient of fluorescent drug analogues from the absorption spectroscopy data. The path length of 10 mm for the photon travelled in the cuvette was taken for analytical measurement with the permittivity in glass medium.

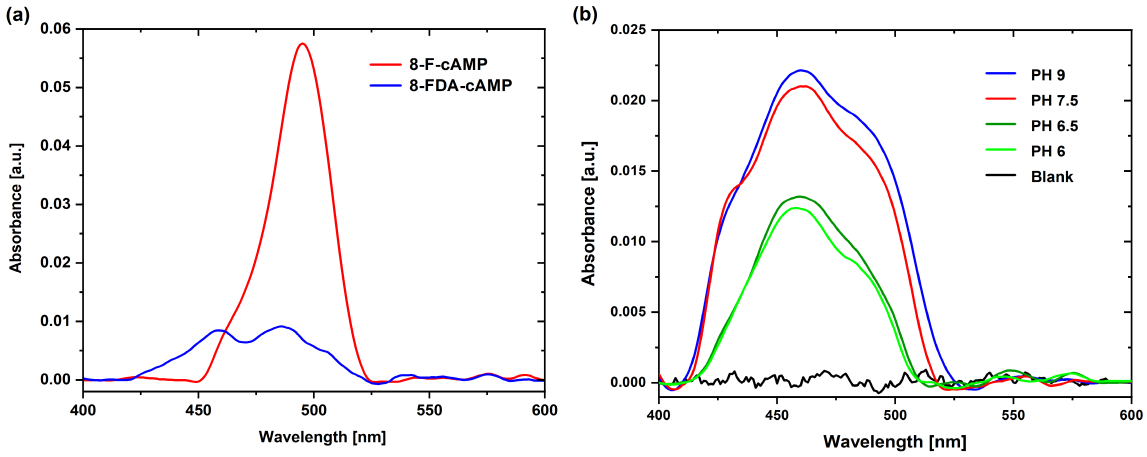

Figure 3.2: Absorbance of 8-F-cAMP and 8-FDA-cAMP molecule: (a) Absorption spectra of fluorescent analogues, where absorbance of each molecule shown with respect to the wavelength ($\lambda_{ex} = 470\ nm$). (b) The absorption maxima of the 8-FDA-cAMP molecule corresponding to the pH 6, 6.5, 7.5 and 9 respectively.

The absorbance of the pre-activated state for the 8-FDA-cAMP molecule (the molecule in the inactivated state), was also measured at a concentration of 1 µM in TRIS buffer, pH 8. Although no absorbance was expected in the non-activated state of the 8-FDA-cAMP molecule, a peak was seen in the absorption spectrum of the molecule as shown in Figure 3.2 (a). Based on the findings, it was determined that a portion of the 8-FDA-cAMP molecule was in pre-activated state. In addition, the absorption spectrum of the 8-FDA-cAMP molecule was measured in TRIS buffer at pH 6, 6.5, 7.5 and 9, respectively [Jokic et al., 2012]. From the above analysis, the pH-dependent pre-activated state of the 8-FDA-cAMP molecule was observed (Figure 3.2 (b)).

3.2 Measurement of fluorescence

In Section 3.1, the extinction coefficient of fluorescent drug analogues was obtained by measuring the absorption spectrum. The emission intensity and quantum yield of fluorescence drug analogues can be determined by the measurement of their emission spectrum. The emission spectra of fluorescein, 8-F-cAMP, MAN194 and AG3457-activated were obtained by steady-state fluorescence spectrometry. The FluoroMax Steady State Spectrofluorometer (HORIBA Scientific) was used for measurements [Section 2.3]. A quartz cuvette (Hellma Analytics) with a path length of 3×3 mm was used. The slit width of the instrument was maintained at 5 nm with an integration time of 1 s during the measurement to obtain an adequate signal-to-noise ratio during the measurement. The absorbance results were obtained from the experimental data after noise reduction optimization. A nominal concentration of 1 μM of each fluorescent sample was used for the analysis. Finally, the solution of 100 µL is taken in a microcuvette for the experiment. At an excitation of 450 nm, emission in the range (from 470-650) nm was observed. Similarly, at 550 nm emission, the excitation in the range of 300-550 nm was measured.

The emission and excitation spectra of 4 distinct compounds were obtained in this experiment with fluorescein as a control. All measurements employed identical experimental conditions, which means that the emission (for excitation spectra) and excitation (for emission spectra) wavelengths were the same. The data sets were plotted on the same scale to get a clear indication of the ratio of change in intensity concerning the wavelength, as shown in Figure 3.3. It can be seen from the figure that the excitation and emission intensity of AG3457-activated is 20% lower than that of fluorescein; however, the intensity of 8-F-cAMP and MAN194 is almost ten times lower than that of fluorescein. Despite the the 8-F-cAMP molecule's high absorption, significantly lower fluorescence intensity was received from the experiment. From the above analysis, we can conclude that the 8-F-cAMP molecule experiences a reduced quantum yield with respect to fluorescein. Although the extinction coefficient of MAN194 is higher than that of AG3457-activated, the emission intensity of MAN194 was significantly lower than that of AG3457-activated, which also indicates a lower quantum yield of the MAN194 molecule.

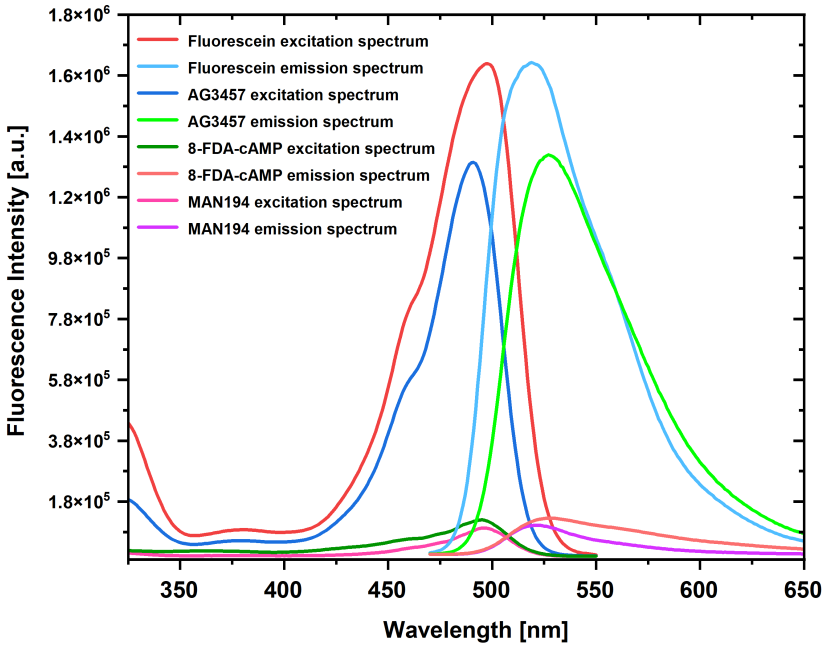

Figure 3.3: Measuring the fluorescence of fluorescent drug analogues: This diagram shows the excitation and emission spectra of fluorescein, 8-F-cAMP, MAN194 and AG3457-activated molecules at 5-nm band-pass obtained by 450 nm excitation and scanning the emission with 1-s integration in the range from 470 to 650 nm.

3.3 Measurement of fluorescence lifetime

After obtaining the optimal spectral characteristics of the novel fluorescent drug analogues, time-resolved information and the excited state lifetime of the drugs were acquired. HORIBA FluoroMax TCSPC Lifetime Fluorometer (HORIBA Scientific) was employed to measure the lifetime of the fluorescent drug analogues as described in Figure 2.6. To calculate the lifetime of the fluorescein, 8-F-cAMP, MAN194, and AG3457-activated, a minimal concentration of 1 µM of each fluorescent sample was taken. The sample was diluted in the TRIS buffer of pH 8 for the final measurements. A quartz cuvette (THORLABS) of light path 10 mm was used in the Fluorometer. The excitation source was a pulsed laser diode (DeltaDiode HORIBA Scientific) with picosecond pulse and repetition rate of 100 MHz. At an excitation pulse of 405 nm, the emission was observed at 520 nm respectively. 0.01% of diluted ludox in the TRIS buffer at pH 8 was applied to extract the measurement instrument response function (IRF). The sensitivity of photon counting of the detector "α" value was maintained below 2% to avoid photon pileup. Fluorescence decay data for the drug analogues were obtained under the same experimental conditions equivalent to the instrument response function (IRF). To obtain the fluores-

cence lifetime, the decay data were deconvoluted with the instrument response function (IRF) to filter out the background noise. The deconvolution of the lifetime decay data was performed with the help of DA6 software (HORIBA Scientific). After the convolution with IRF, we fitted the decay data with the exponential decay function to acquire the lifetime of the fluorescent sample. The exponential fit function was selected for each decay depending on the best fit parameter.

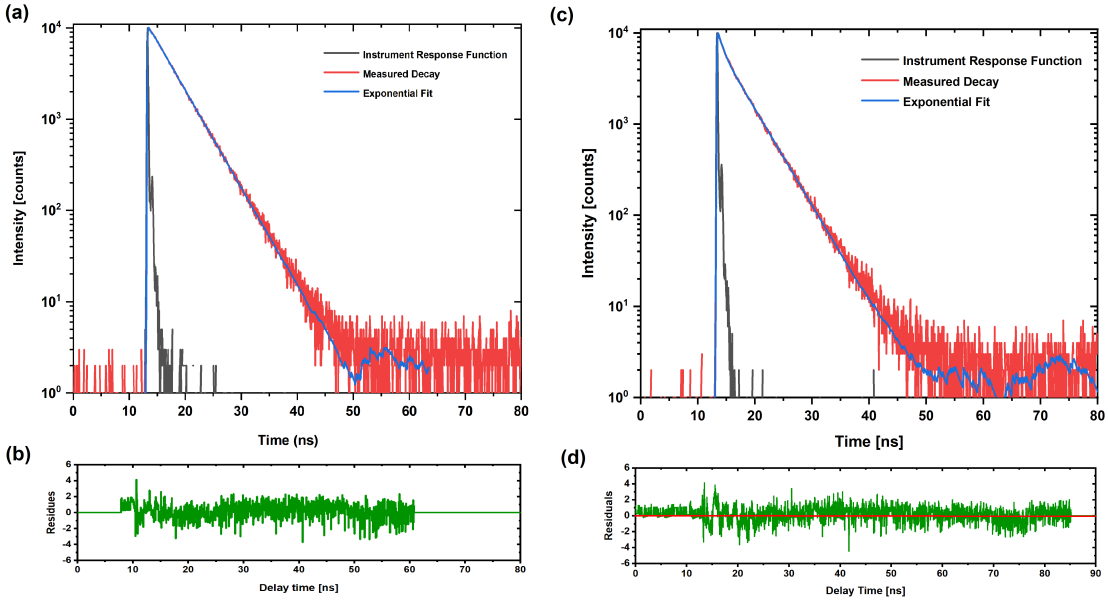

Figure 3.4: The fluorescence lifetime of fluorescein and 8-F-cAMP: Fluorescence lifetime of (a) fluorescein and (c) 8-F-cAMP molecule. The black line represents the instrument response function (IRF), the red is the observed fluorescent decay curve from the TCSPC experiment, and the blue is for the exponential fit. For the fluorescein and 8-F-cAMP molecule, the data was deconvoluted with the IRF and then fitted with the double exponential decay fit function as shown by the blue line in Figure (a), (c). The residuals for the double exponential fitted function of fluorescein and 8-F-cAMP are shown in (b) and (d), respectively.

The equation for a double exponential decay fit is as follows:

$$F(t) = A + B_1\, exp\frac{-t}{\tau_1} + B_2\, exp\frac{-t}{\tau_2} \tag{3.1}$$

In the case of double exponential fit, the lifetime τ_1 corresponds to scattering. However, the lifetime τ_2 correlate with the lifetime of the fluorescent sample. The triple exponential decay fit equation can be written as,

$$F(t) = A + B_1\, exp\frac{-t}{\tau_1} + B_2\, exp\frac{-t}{\tau_2} + B_3\, exp\frac{-t}{\tau_3} \tag{3.2}$$

In the triple exponential fit, the lifetime τ_1 corresponds to scattering. However, the lifetime τ_2 and τ_3

correlate with the lifetime of the fluorescent sample.

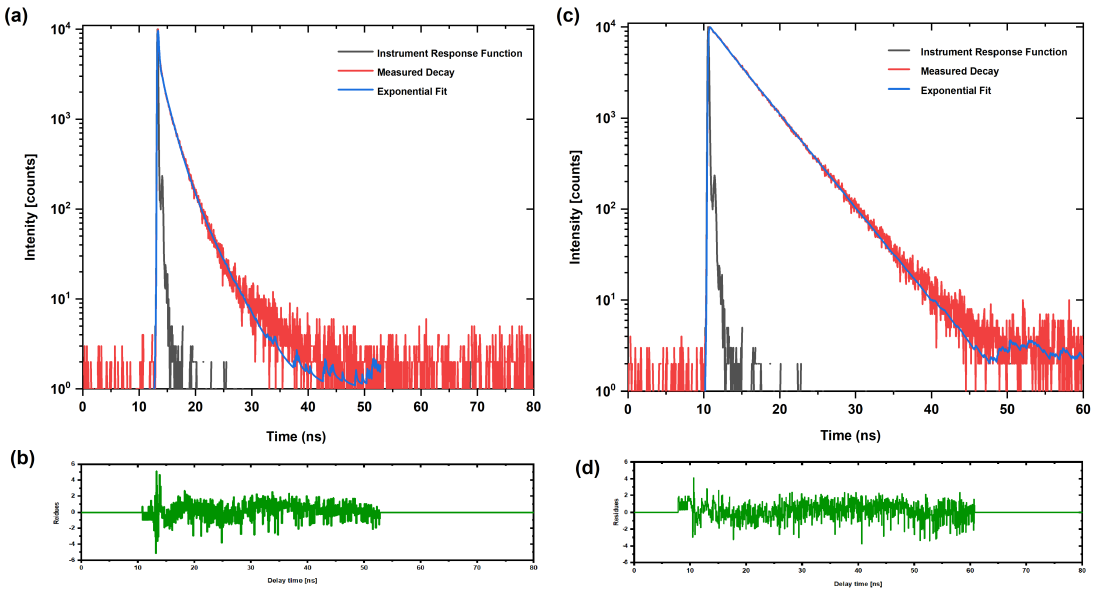

Figure 3.5: The fluorescence lifetime of MAN194 and AG3457-activated: Fluorescence lifetime of (a) MAN194 and (b) AG3457-activated molecule. The black line represents the instrument response function (IRF), the red is the observed fluorescent decay curve from the TCSPC experiment, and the blue is for the exponential fit. For the MAN194 molecule, the data was deconvoluted with the IRF and then fitted with the triple exponential decay fit function as shown by the blue line in Figure (a). however, in the case of AG3457-activated, the data was fitted with the double exponential fit function as shown by the blue line in Figure (c). The residuals for the exponential fitted function of MAN194 and AG3457 are shown in (b) and (d), respectively.

The fluorescence decays of all fluorescent drug analogues were acquired on a time-resolved spectrofluorometer. Then, the decay data were analyzed and deconvoluted by DA6 software (HORIBA Scientific). As discussed previously, a minimum of double exponential decay components was required to describe the fluorescence decay of fluorescein, 8-F-cAMP and AG3457-activated, whereas that of MAN194 was well described by a triple exponential model. The results of the fittings are shown in Figure 3.4 & 3.5. The fitting criterion for MAN194 was significantly improved by adding a triple component to the model (from χ^2 = 23.733 to χ^2 = 1.214). The data for the lifetime is fitted with the double exponential decay function yielding the goodness of fit parameter χ^2 of 1.21 as shown in Figure 3.4. The acquired lifetime of fluorescein was 4.01 ns, whereas the obtained lifetime of the 8-F-cAMP molecule was 4.08 ns. The obtained lifetimes for MAN194 were 1.51 ns and 3.41 ns, respectively. Similarly, the lifetime of AG3457-activated was obtained as 4.18 ns with the double exponential decay fit (Figure 3.5(b)). The above results show that the lifetimes of fluorescein, 8-F-cAMP and AG3457-activated are almost similar; however, the average lifetime of MAN194 is 2.46 ns.

3.4 Measurement of steady-state anisotropy

In the previous sections the spectra, absorbance, and lifetime of novel fluorescent drug analogues were discussed. Initially, the optimal spectral properties of the drug analogues were obtained. After assessing the spectral properties of drug analogues, an in vitro experiment was performed to determine the drug's binding to a protein. Then we set to evaluate the saturation binding of purified proteins to our novel drug analogues using steady state fluorescence anisotropy. In the saturation binding experiment, a the steady-state Horiba spectrofluorometer was employed to measure the steady-state anisotropy. Once again, we used fluorescein as a control for this experiment.

The initial stock solution of the protein was 3 μM and then diluted in the TRIS buffer of pH 8 with a ratio of 1:3 to get the final concentration of 1 μM. For the saturation binding of fluorescein, a minimal concentration of 10 nM of the compound was used during the experiment. First, the steady-state anisotropy of fluorescein was obtained in the TRIS buffer at pH 8. Then, the increasing concentration of purified protein was added with fluorescein and measured steady-state anisotropy was observed in each step. The final concentrations of the protein in the experiment were 10 nM, 50 nM, and 100 nM, respectively. Similarly, the concentration of 50 nM of MAN194 was used with the increasing concentration of purified protein for the saturation binding experiment.

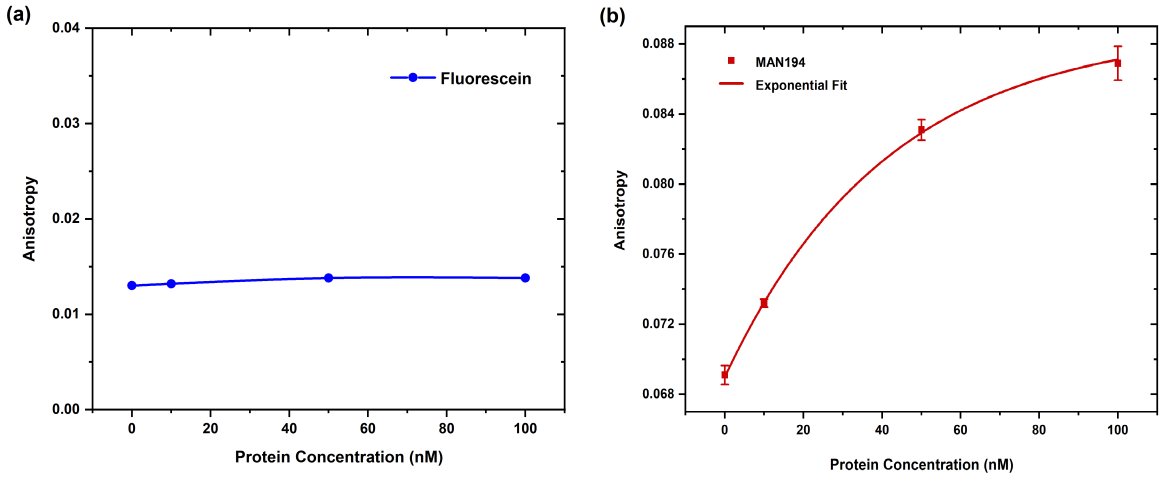

Figure 3.6: Saturation binding of fluorescein and MAN194: (a) Steady-state anisotropy of fluorescein with the increasing protein concentration, (b) The data point represents the Steady-state anisotropy of MAN194 by the increasing protein concentration with standard deviation error bars and the red line is for exponential fit.

From Figure 3.6(a), it can be seen that with the increase in protein concentration, the steady-state anisotropy for fluorescein remains the same, consistent with the assumption that fluorescein does not bind to this purified protein. Whereas, from the saturation binding curve of MAN194 (Figure 3.6 b), one can perceive that with the increase of protein concentration, the value for the steady-state anisotropy was increased. Four experiments were performed with the same experimental conditions for the saturation binding of MAN194 and plotted the average data with error bars as represented in Figure 3.6(b). The data were fitted with the saturation binding function (sigmoid function) and acquired the dissociation binding constant $K_D = 50n$M.

The absorbance, lifetime and steady-state anisotropy of novel fluorescent drug analogues were obtained by fluorescence spectroscopy experiment. The summary for the spectroscopic characterization of the drug analogues is given in Table 3.3. From the table, it can be seen that with the increase in steady-state the fluorescence lifetime decreases and vice-versa.

Molecule	Absorbance	Fluorescence lifetime	Steady-state anisotropy
Fluorescein	0.058	4.01 ns	0.011
8-FDA-cAMP	0.059	4.08 ns	0.023
MAN194	0.029	1.51 ns, 3.41 ns	0.057
AG3457-activated	0.018	4.18 ns	0.016

Table 3.3: Table for the measurement of absorbance, fluorescence lifetime and steady-state anisotropy of fluorescent drug analogues.

3.5 Measurement of time-resolved anisotropy by TCSPC

The HORIBA FluoroMax TCSPC experimental setup was then employed to measure time-resolved anisotropy. The concentration of 1 μM for each drug analogue was used for the measurement purpose. For the measurement objective, 1 μM concentration for each drug analogue was diluted in TRIS buffer (pH 8) and used 0.01% of diluted ludox to measure the instrument response function (IRF). The G-factor of the instrument was obtained as 0.68. For the measurement of the G-factor, the sample was excited with a horizontally polarized light, and we observed the horizontal and vertical intensity of the emission light. The ratio of the intensity from the horizontal to vertical is known as the G-factor of the instrument. The fluorescence decay data for the intensity parallel and intensity perpendicular

component was acquired. The data is then fitted with the double exponential decay function to obtain the time-resolved anisotropy and rotational diffusion time of the fluorescent drug analogues.

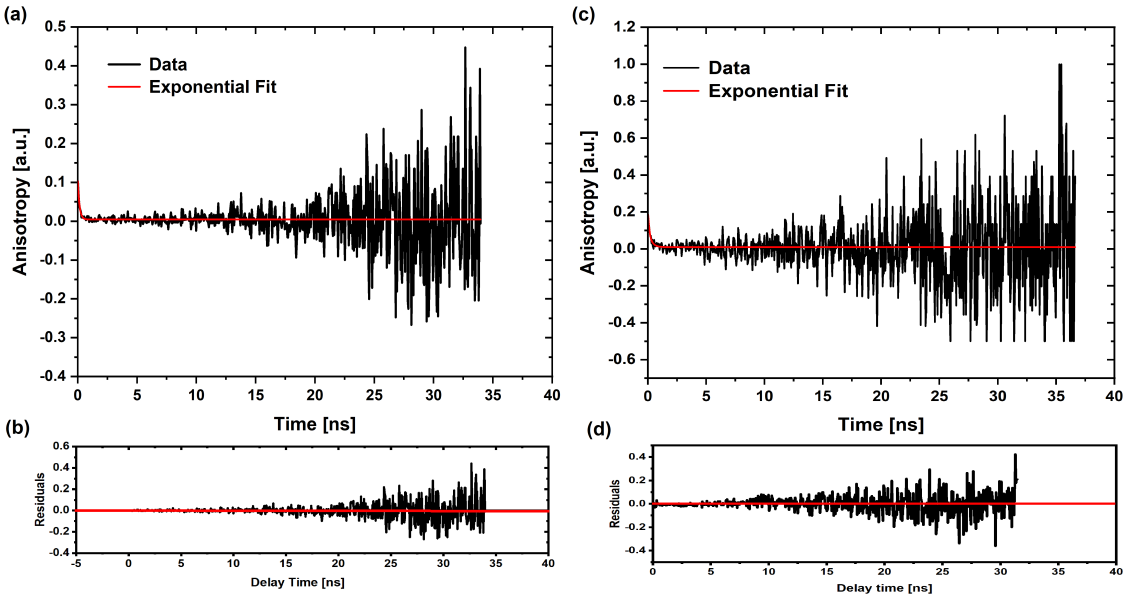

Figure 3.7: Time-resolved anisotropy of fluorescein and 8-F-cAMP molecule: Time-resolved anisotropy of (a) fluorescein and (c) 8-F-cAMP molecule diluted in TRIS buffer.The black line represents the observed fluorescent decay curve from the TCSPC experiment and the data is deconvoluted with the IRF and then fitted with the double exponential decay fit function as shown by the red line. The residuals for the exponential fit of MAN194 and 8-F-cAMP molecules are shown in (b) and (d), respectively.

Having acquired the fluorescence decay data of drug analogues of 1 μM diluted in TRIS buffer as represented in Figure 3.7 and 3.8 respectively. Then the anisotropy data is fitted with an exponential decay function to obtain the value for the rotational diffusion time of the drug analogues. The value of χ^2 obtained for this fitting is 1.24. The equation for the time-resolved anisotropy was given by [Lee et al., 2011]

$$R_t = R_\infty + (R_0 - R_\infty)\, e^{-\frac{t}{\tau}} \tag{3.3}$$

Where R_0 stands for the anisotropy at t=0, R_∞ is the anisotropy when $t = \infty$ and τ represents the rotational correlation time. The parameters obtained for fluorescein after fitting the exponential function with the decay data (Figure 3.7(a)) are $R_0 = 0.11 \pm 0.02$, $R_\infty = 0.04 \pm 0.01$ and the rotational diffusion time $\tau = 0.14 \pm 0.04$ ns. Similarly, for 8-F-cAMP we obtained the anisotropy and rotational diffusion time are $R_0 = 0.18 \pm 0.04$, $R_\infty = 0.08 \pm 0.01$ and $\tau = 0.19 \pm 0.06$ ns (Figure 3.7 c). For MAN194 and

AG3457-activated molecule the data obtained from the time-resolved were anisotropy were fitted with triple and double exponential decay fir function as represented in Figure 3.8. The obtained anisotropy of $R_0 = 0.41 \pm 0.04$, $R_\infty = 0.015 \pm 0.007$ and the rotational diffusion time $\tau = 0.39 \pm 0.02$ ns for MAN194 molecule (Figure 3.8 a). Similarly, for AG3457-activated molecule the obtained tim-resolved anisotropy and rotational diffusion time were $R_0 = 0.18 \pm 0.42$, $R_\infty = 0.011 \pm 0.002$ and $\tau = 0.22 \pm 0.18$ ns respectively.

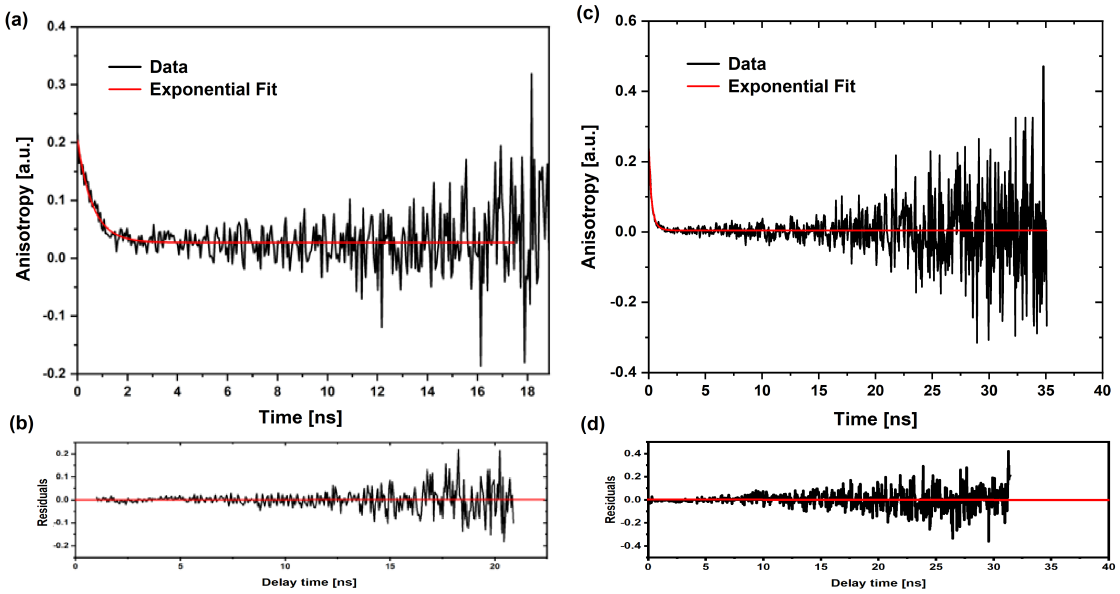

Figure 3.8: Time-resolved anisotropy of MAN194 and AG3457-activated molecule: Time-resolved anisotropy of (a) MAN194 and (c) AG3457-activated molecule diluted in TRIS buffer.The black line represents the observed fluorescent decay curve from the TCSPC experiment and the data is de-convoluted with the IRF and then fitted with the double exponential decay fit function as shown by the red line. The residuals for the exponential fit of MAN194 and AG3457-activated molecules are shown in (b) and (d), respectively.

From the above data, it can be observed that the rotational diffusion time of both 8-F-cAMP and MAN194 molecules were higher than that of the fluorescein, consistent with their larger molecular weight. On the other hand the behaviour of time-resolved anisotropy for 8-F-cAMP and AG3457-activated molecule was almost similar, consistent with the notion that the fluorescein tag increases the rotational diffusion time of the molecule.

Chapter 4

Quantifying the cellular uptake of fluorescent drug analogues

4.1 Cellular uptake kinetics of FDA, 8-FDA-cAMP and drug analogues

The spectroscopic properties of drug analogues have been acquired in the previous section. The current chapter will discuss how to visualize and study the intracellular behaviour of fluorescent drug analogues, with a particular focus on the cellular and subcellular uptake kinetics of the fluorescent drug analogues. A laser scanning confocal microscope (Leica TCS SP8) was employed to monitor the cellular uptake kinetics of drug analogues. The HEK293T cells, a well established model for in-vitro studies, is used throughout. The cells were cultured in a 2D 8-Well Ibdi imaging slides (μ-Slide 8 Well high) with DMEM culture medium (Glucose, Sodium pyruvate, L-Glutamate and $NaHCO_3$) for imaging. Ibidi microscopy slides have a polymer coverslip bottom with the highest optical quality and are thus suitable for wide range of microscopy techniques (e.g., widefield fluorescence, confocal microscopy, two-photon microscopy, FRAP, FRET and FLIM).

The objective of this work was to monitor the cellular uptake of the drug analogues in the different compartments of HEK293T cells using the increase of Fluorescein signal as FDA's ester bonds are cleaved by intracellular esterases. To monitor the subcellular import kinetics of our drug analogues, the HEK293T cells were labelled with DAPI ($4', 6 - diamidino - 2 - phenylindole$) and MitoTracker far-red dye as a reference. The DAPI dye ($\lambda_{abs}/\lambda_{em} \sim 405/488nm$) was used for labelling the nucleus of the cells,

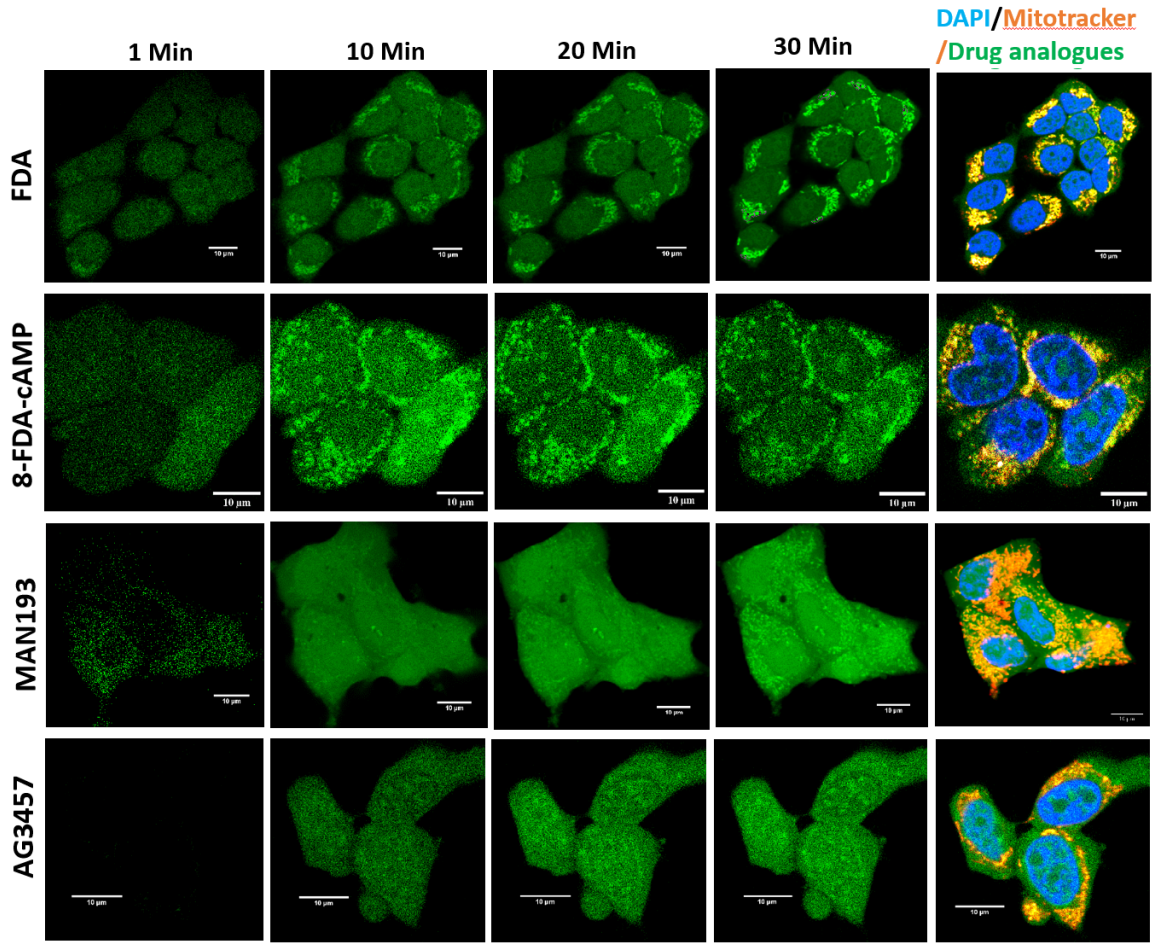

Figure 4.1: Real-time cellular uptake image: Real-time confocal images of HEK293T cells incubated with FDA (C = 1 μM), 8-FDA-cAMP (C = 10 μM), MAN193 (C = 1 μM) and AG3457 (C = 1 μM) at 37 $°C$. The green color for each time frame image represents the uptake kinetics of the drug analogues. The HEK293T cells are preincubated with MitoTracker (mitochondria) and DAPI (nucleus) dyes represented by the orange and blue colors in the figure respectively. The pixel width of each image obtained in a similar context is represented by the scale bar of 10 μm displayed on each image.

whereas, MitoTracker far-red dye ($\lambda_{abs}/\lambda_{em} \sim 644/665nm$) was used for the labelling of mitochondria. Before imaging, the cell culture medium was washed out from the 8-Well Ibidi slide and stained the cells with 50 nM of MitoTracker deep red and DAPI in a DMEM cell culture medium for 20 Minutes. After 20 min, the Ibidi slide was washed with an HBSS buffer of pH 7.3 ($+CaCl_2 + MgCl_2$) three times to ensure the cleaning of the culture medium to get less background noise. Then, the coverslip was mounted into the temperature chamber of the microscope by maintaining 37 $°C$ and 5% CO_2. A temperature-controlled chamber was used to keep the cells in a lively environment during long-term live-cell imaging. The imaging was done in the HBSS medium ($+CaCl_2 + MgCl_2$) and with the

imaging condition of 85 nm resolution. Confocal time-series live-cell imaging was performed on the HEK293T cell line with the same imaging conditions as that of the optimum spectral characteristics of drug analogues ($\lambda_{abs}/\lambda_{em} \sim 485/520nm$). The interval between each frame was maintained at 1 min and at the time frame of 5 min, the fluorescent compound was added to the imaging chamber to observe the uptake kinetics of the fluorescent drug analogues into the cells.

The fluorescein diacetate (FDA) compound has been used for small molecule labels and becomes fluorescent when hydrolyzed in the cellular environment by intracellular esterases. The cellular uptake kinetics of 8-FDA-cAMP, MAN193 and AG3457 molecules were observed and FDA was treated as a control for this experiment. After obtaining fluorescence microscopy images (or time-lapse movies) of drug analogues, the uptake of the drugs into the different compartments of the cells was quantified, within the possibility offered by the resolution of confocal microscopy. Figure 4.1 represents the cellular uptake kinetics of drug analogues on HEK293T cells at different time points. The green color represents the uptake of the drug analogues; however, the blue represents the nucleus and the orange one for the mitochondria. From Figure 4.1, the subcellular localization of FDA, 8-FDA-cAMP and MAN193 molecules was observed in the HEK293T cells. Besides fluorescence microscopy studies, the intercellular distribution of drugs has also been quantified using fluorescence microscopy data. The data obtained by fluorescence microscopy were analyzed by Fiji software to quantify the subcellular import kinetics of the drug analogues. For the analysis purpose, the intensity of mitochondria, nucleus, and cytosol for each cell was quantified in the time frame by selecting the random region of interests (ROIs). After obtaining the intensity of different ROIs for each time frame with a standard deviation, the normalized data were plotted concerning the time axis as shown in Figure 4.2. The scale bar mentioned in each image represents a pixel width of 10 μm. The subcellular import kinetics of FDA, 8-FDA-cAMP, MAN193 and AG3457 were obtained for each frame of the movies, although no subcellular localization was observed in the case of the AG3457 molecule.

Figure 4.2(a) shows the uptake kinetics of the FDA, 8-FDA-cAMP, MAN193 and AG3457 drugs into the different cell compartments. FDA, MAN193 and AG3457 molecules were added to the HBSS imaging medium with 0.01% DMSO concentration, however, the 8-FDA-cAMP molecule was used at 0.5% DMSO concentration. The kinetic model has been used to describe the membrane penetration and distribution of drug analogues into the distinct organelles of cells. The kinetic models explain the uptake rate of the drugs into the cellular environment and the binding of the compound in each particular re-

gion of interest. It can be observed from Figure 4.2(a), that the kinetics of uptake of the drug analogues to the cytosol, nucleus and mitochondria of cells. Especially, our interest was to understand the uptake of the drug analogues in the region of mitochondria. The MitoTracker far-red dye uptake kinetics was used as a control for this experiment. The behaviour of the uptake kinetics of each drug was different. The kinetics of uptake of fluorescein diacetate was fast, whereas the kinetics of uptake of MAN193 and AG3457 drugs were quite slow when compared to FDA. We ascribe the peak observed in the traces of FDA and 8-FDA-cAMP molecule to the effect of dimethyl sulfoxide on cell membrane permeability, as will be discussed in more detail later. Figure 4.2(b) represents the kinetics of uptake of drug analogues into the cell with error bars.

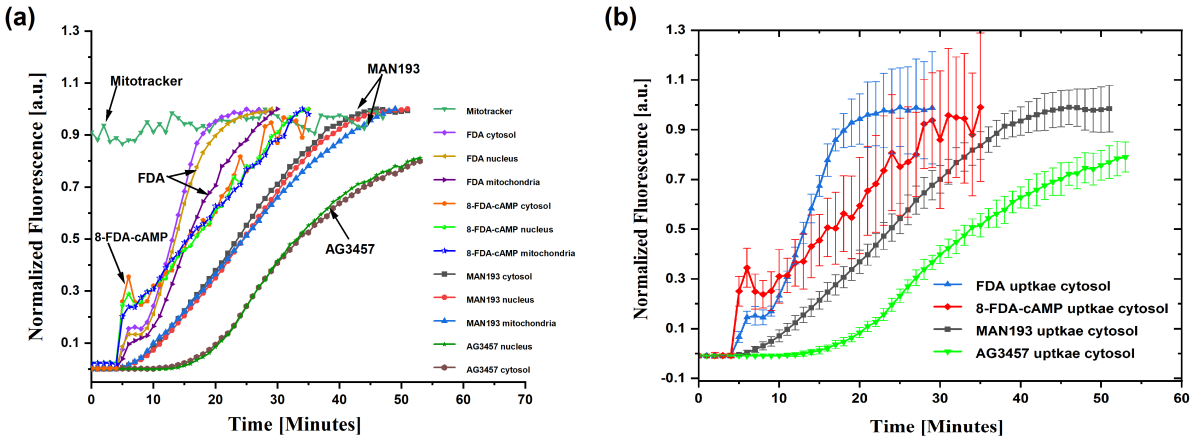

Figure 4.2: Cellular uptake kinetics plot: Cellular uptake kinetics of drug analogues on HEK293T cells. (a) Cellular uptake kinetics of FDA (C = 1 µM), 8-FDA-cAMP (C = 10 µM), MAN193 (C = 1 µM) and AG3457 (C = 1 µM) measured by confocal microscopy. The KEK293T cells are used for the experiment with the imaging medium of HBSS ($+CaCl_2 + MgCl_2$) incubated at 37 $^{\circ}C$ on microscopy slide. Each data points on uptake kinetics curve represent the real-time mean normalized confocal image intensities of the drugs into the cytosol, nucleus and mitochondria of the cells from 9 randomly selected ROIs. (b) The cellular uptake kinetics of the drugs into the cytosol with error bars measured from the standard deviation of mean intensities for different cells. The error bars of each data point represents the stand deviation of uptake intensity for each time point acquired from the experiment.

4.2 Subcellular localization and competition binding experiment of MAN193 molecule preincubated with MAN164

In the Section 4.1, the saturation binding and cellular uptake kinetics of the drug analogues are obtained by live-cell confocal microscopy experiment. This experiment aimed at observing the uptake kinetics

of our drug analogues by a competition binding experiment and to measure the binding of a labelled drug in the presence of various concentrations of the unlabelled drug. From the uptake kinetics experiment of our drug analogues, the subcellular localization of the drugs into the intercellular sites was determined. The purpose of this experiment was to conclude the binding sites of our drug in the different compartments of the cells and to identify the binding sites of the drug analogues. Consequently, the cells were preincubated with a competitor drug, which preoccupied the binding sites of the drug analogues.

The competition binding of MAN193 molecule with the preincubation of MAN164 is discussed in this section. At first, the HEK293T cells were preincubated with MAN164 of 1 μM for 20 min in HBSS buffer ($+CaCl_2 + MgCl_2$) at pH 7.3. Then obtained the live-cell confocal time-series experiment by adding the MAN193 drug of 1 μM into the imaging chamber. From Figure 4.3(a), we can observe the real-time confocal images of HEK293T cells incubated with MAN193 (C = 1 μM), and MAN193 (C = 1 μM) preincubated with MAN164 (C = 1 μM) at 37 $^{\circ}C$. The HEK293T cells were used for the experiment with the imaging medium of HBSS ($+CaCl_2 + MgCl_2$) with 0.01% DMSO on a microscopy slide. The green color for each time frame image represents the uptake kinetics of the drug analogues. The HEK293T cells were preincubated with MitoTracker (mitochondria) and DAPI (nucleus) dyes represented by the orange and blue colors in the figure respectively. The fluorescent intensities were measured of each frame for the cellular uptake kinetics of the drug analogues. The Fiji software was used to obtain the intensity of each frame by selecting some random ROIs in the mitochondrial region. Figure 4.3(b) depicts the cellular uptake kinetics plot for MAN193 drug into the mitochondrial region of the cell with or without preincubation with MAN164 . The subcellular localization of MAN193 in the cytosolic region is shown in Figure 4.3(a); however, no subcellular localization observed in the case of preincubation with MAN164.

For the analytical measurement of the subcellular localization of MAN193 on HEK293T cells with or without preincubation of MAN164, the standard deviation and variance for different uptake time points were measured. After normalizing the image pixel intensities, the standard deviation and variance were obtained by selecting 4 random ROIs in the cytosolic region of the cells, as shown in Figure 4.3(c). Equation 4.1 represent the measurement of the standard deviation and variance from the mean pixel intensities.

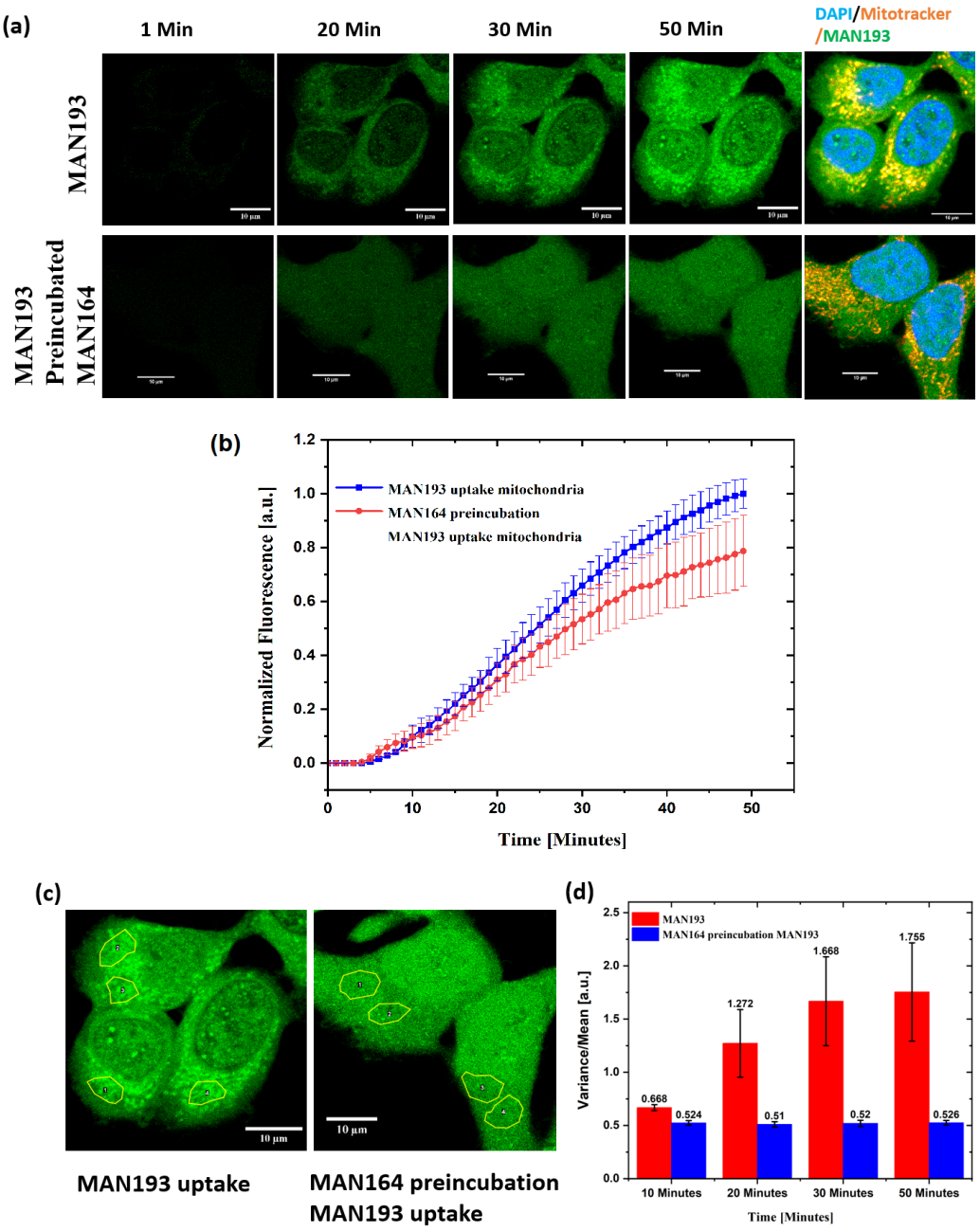

Figure 4.3: Competition binding experiment of MAN193 molecule preincubated with MAN164: (a) Real-time confocal images of HEK293T cells incubated with MAN193 (1 μM) preincubated with MAN164 (C = 1 μM) at 37 $^{\circ}C$. The green color for each time frame image represents the uptake kinetics of the drug analogues. The HEK293T cells are preincubated with MitoTracker (mitochondria) and DAPI (nucleus) dyes represented by the orange and blue colors in the figure respectively. (b) Cellular uptake kinetics of MAN193 (C = 1 μM) preincubation with MAN164 (C = 1 μM) uptake on HEK293T cells. (c) Measurement for the subcellular localization of MAN193 uptake & MAN164 preincubation, MAN193 uptake at 1 μM. (d) The diagram represents the bar chart for the variance/mean calculation for the subcellular localization and completion binding experiment plotted with different time points.

$$\sigma^2 = \frac{\sum_{i=1}^{N}(x_i - \mu)^2}{N} \tag{4.1}$$

To analyze the subcellular localization, the variance above the mean was measured for analyze the clustering of the image pixel intensities in the cytosolic region of the cells. The variance versus mean ratio characterizes the distribution of objects in a given area of space. To observe the distribution of image pixel intensities in the cytosolic region of the cells, the variance versus mean was obtained as shown in equation 4.2.

$$Variance/Mean = \sigma^2/\mu = \frac{\sum_{i=1}^{N}(x_i - \mu)^2}{\sum_{i=1}^{N} x_i} \tag{4.2}$$

Where μ stands for the mean pixel intensity.

The variance across the mean intensities of 4 randomly chosen ROIs was selected for uptake of MAN193 into the cells with or without preincubation of MAN164. The plotted data was then placed in a bar chart as shown in Figure 4.3(d). From the figure it can be seen that the variance over the mean ratio for MAN193 uptake remains constant with increasing uptake time points, but the variance over the mean ratio for MAN193 preincubated with MAN164 increases with uptake time. From the above results we infer the subcellular localization of drug analogues in the mitochondrial region of cells. Although, the discussed experiment didn't confirm the specific binding site in this region and to determine the exact binding sites, a high-resolution expansion microscopy setup was required.

The variance over the mean intensities was recorded exclusively in cytosolic portion (outside the region of the mitochondria) of the cells to obtain control for this experiment. The variance from the mean was examined by selecting 4 random ROIs in the pure cytosolic region and plotting them in a bar graph as shown in Figure 4.4. From the figure it can be observed that the variance above the mean remains consistent for uptake of drug MAN193 with or without preincubation of MAN164. From the above analysis we inferred the subcellular localization of our drug analogs in the subcellular compartment of cells.

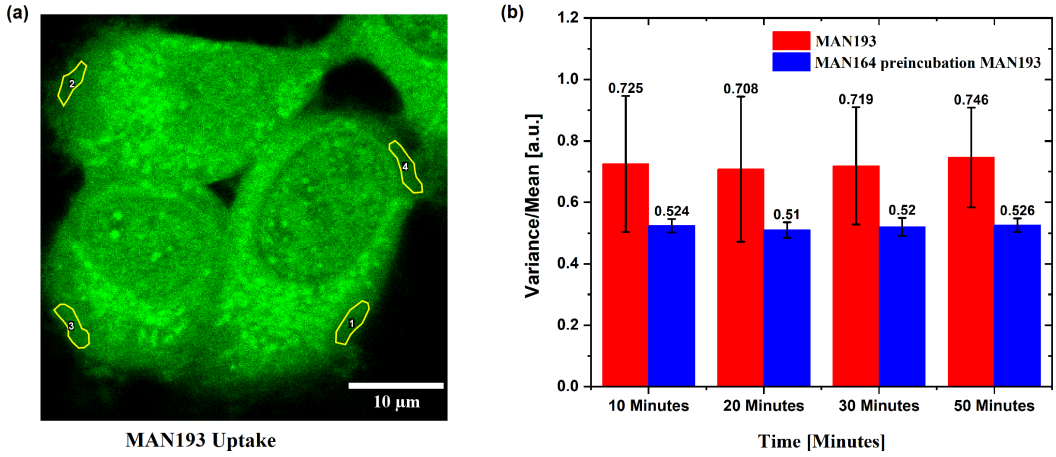

Figure 4.4: Control for the competition binding experiment of MAN193 molecule preincubated with MAN164: (a) Measurement for the subcellular localization of MAN193 uptake & MAN164 preincubation, MAN193 uptake at 1 µM concentration. For each experiment the mean, and standard deviation & variance are calculated from the normalized pixel intensities of 4 randomly oriented ROIs from the pure cytosolic region by refraining from the region of mitochondria of cells. (b) The diagram represents the bar chart for the variance/mean calculation for the subcellular localization and completion binding experiment plotted with different time points.

4.3 Subcellular localization and competition binding experiment of 8-FDA-cAMP molecule preincubated with 8-Br-cAMP molecule

The competition binding experiment of MAN194 molecule preincubation with MAN164 is discussed in Section 4.2. Similarly, this work explains the competition binding experiment of 8-FDA-cAMP [Bock et al., 2020] of 10 µM with preincubation of 8-Br-cAMP of 1 µM on HEK293T cells.

For the competition binding experiment, 1 µM of 8-Br-cAMP was preincubated in HEK293T cells for 20 min in HBSS buffer ($+CaCl_2 + MgCl_2$) at pH 7.3. Then, the live-cell confocal time-series experiment was performed by adding the 8-FDA-cAMP drug of 10 µM into the imaging chamber. The HEK293T cells were used for the experiment with the imaging medium of HBSS ($+CaCl_2 + MgCl_2$) with 0.05% DMSO on a microscopy slide. The green color in each time frame image represents the uptake kinetics of the drug analogues. The HEK293T cells were preincubated with MitoTracker (mitochondria) and DAPI (nucleus) dyes represented by the orange and blue colors in the figure, respectively. The fluorescence intensities were measured in each frame for the cellular uptake kinetics of the drug analogues. The Fiji software was used to obtain the intensity of each frame by selecting some random ROIs in the mitochondrial region. Figure 4.5(b) depicts the cellular uptake kinetics plot for 8-FDA-cAMP drug into

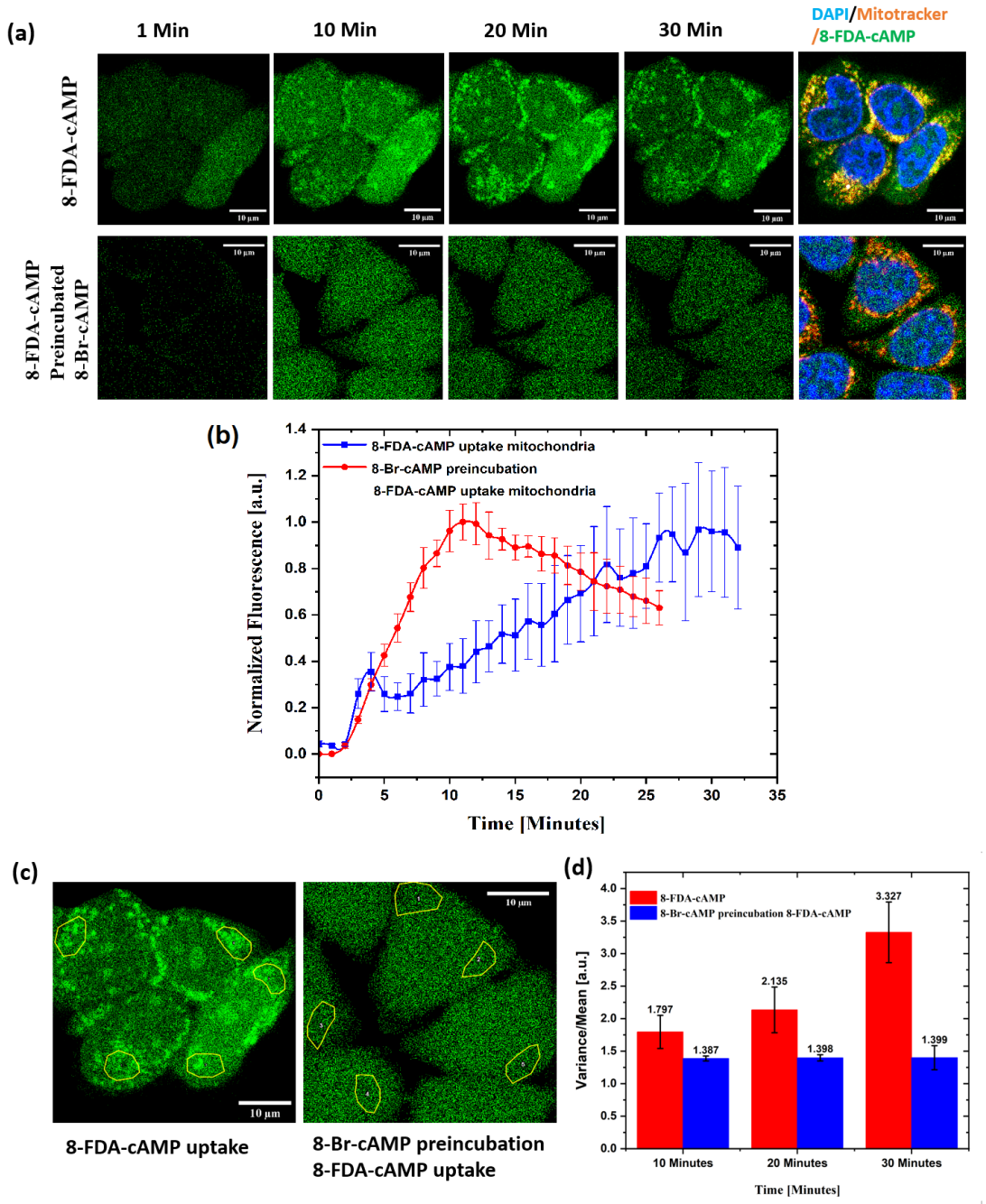

Figure 4.5: Competition binding experiment of 8-FDA-cAMP preincubated with 8-Br-cAMP: (a) Real-time confocal images of HEK293T cells incubated with 8-FDA-cAMP (C = 10 μM) preincubated with 8-Br-cAMP (C = 1 μM) at 37 $^{\circ}C$. The green color for each time frame image represents the uptake kinetics of the drug analogues. The HEK293T cells are preincubated with MitoTracker (mitochondria) and DAPI (nucleus) dyes represented by the orange and blue colors in the figure respectively. (b) Cellular uptake kinetics of 8-FDA-cAMP (C = 10 μM) preincubation with 8-Br-cAMP (C = 1 μM) uptake on HEK293T cells. (c) Measurement for the subcellular localization of 8-FDA-cAMP uptake & 8-Br-cAMP preincubation, 8-FDA-cAMP uptake at 10 μM. (d) The diagram represents the bar chart for the variance/mean calculation for the subcellular localization and completion binding experiment plotted with different time points.

the mitochondrial region of the cell with or without preincubation with 8-Br-cAMP. The subcellular localization of 8-FDAcAMP in the cytosolic region is shown in Figure 4.5(a); however, no subcellular localization was observed in the case of preincubation with 8-Br-cAMP molecule.

For the quantitative assessment of the subcellular localization of 8-FDA-cAMP molecule on HEK293T cells with or without preincubation of 8-Br-cAMP, the standard deviation and variance for different uptake time points were measured. After normalizing the image pixel intensities, the standard deviation and variance were obtained by selecting 4 random region of interests (ROIs) in the cytosolic region of the cells, as shown in Figure 4.5(c). Four random ROIs were selected in the cytosolic region that contained mitochondria.

To analyze the subcellular localization we measured the variance over mean for the clustering of the image pixel intensities in the cytosolic region of the cells. Variance over mean ratio was used to characterize the distribution of objects in the particular region of space, with more variance reflecting a more aggregated pattern/phenotype (Equation 4.2).

The variance across the mean intensities of four randomly chosen ROIs was selected for uptake of 8-FDA-cAMP into the cells with or without preincubation of 8-Br-cAMP molecule. The plotted data was then placed in a bar chart as shown in Figure 4.5(d). From the figure it can be seen that the variance over mean ratio for 8-FDA-cAMP preincubated with 8-Br-cAMP remains constant for increasing uptake time, but the variance over the mean ratio for 8-FDA-cAMP increases with time. From the above results, combined with the microscopic imaging, we corroborate a strong subcellular localization of drug analogues, namely in the mitochondrial region of cells. Although, the discussed experiment didn't confirm the specific binding site in this region and to determine the exact binding sites, a higher-resolution dual-labelling microscopy setup, or specific biochemistry, would be required.

We then measured the variance over the mean of the pixel intensities outside the region of the mitochondria of the cells, in order to assess whether an increased clustering/binding could be observed also in the cytosol. The variance from the mean was examined by selecting four random ROIs in the exclusively cytosolic region and plotting them in a bar graph as shown in Figure 4.6. From Figure 4.6, it can be observed that the variance over the mean ratio remains constant over time, with or without preincubation of 8-Br-cAMP. From the above analysis we further concluded the subcellular localization of our drug analogs in the perimitochondrial region of the cell.

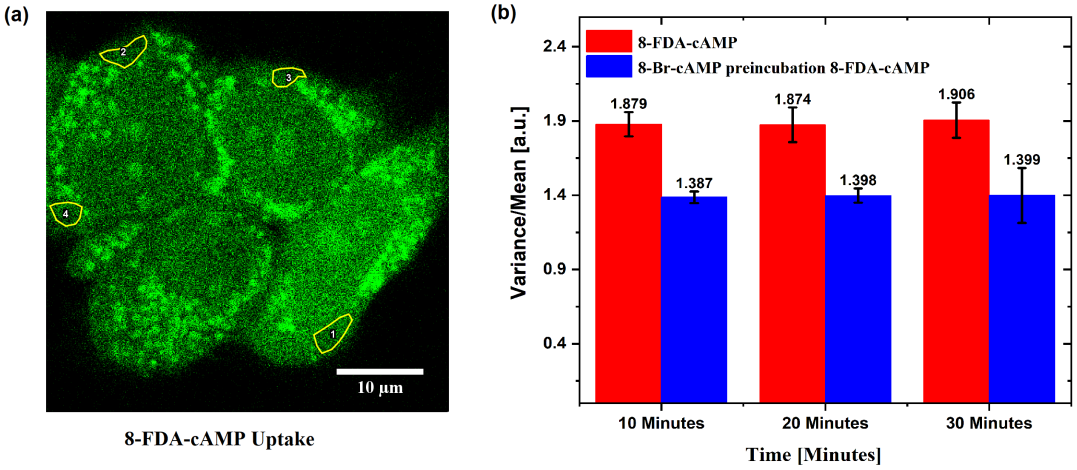

Figure 4.6: Control for the competition binding experiment of 8-FDA-cAMP molecule preincubated with 8-Br-cAMP: (a) Measurement for the subcellular localization of 8-FDA-cAMP uptake & 8-Br-cAMP preincubation, 8-FDA-cAMP uptake at 10 µM concentration. For each experiment the mean, and standard deviation & variance are calculated from the normalized pixel intensities of 4 randomly oriented ROIs from the pure cytosolic region by refraining from the region of mitochondria of cells. (b) The diagram represents the bar chart for the variance/mean calculation for the subcellular localization and completion binding experiment plotted with different time points.

4.4 Effect of dimethyl sulfoxide on the membrane permeability of FDA and 8-FDA-cAMP molecule

The plasma membrane of a cell plays a crucial role in its structural integrity and enables several cellular functions like active transport, cell-cell communication, chemical signal transduction and cell adaptation [Gironi et al., 2020]. In this section, the effect of dimethyl sulfoxide (DMSO) on the lipid bilayer of the cells was investigated. Dimethyl sulfoxide $(CH_3)_2SO$ is a two-carbon sulfoxide with two methyl substituents on the sulfur atom (Figure 4.7 a). As such, DMSO is a small amphiphilic molecule and it is widely used in cell biology to enhance the permeability of larger peptides and drugs through the DPPC membrane [de Ménorval et al., 2012]. DMSO is used as a cryoprotectant and has numerous applications in cell biology. DMSO was synthesized in 1867 by the oxidation of dimethyl sulfide [Yu and Quinn la, 1994], and since the 1960s, this small molecule has been widely used and acts as a chemical penetration enhancer in the lipid bilayer. Several articles ([Notman et al., 2006], [Gurtovenko and Anwar, 2007], [de Ménorval et al., 2012]) have explained the effect of DMSO on permeability by using molecular dynamics and simulation methods.

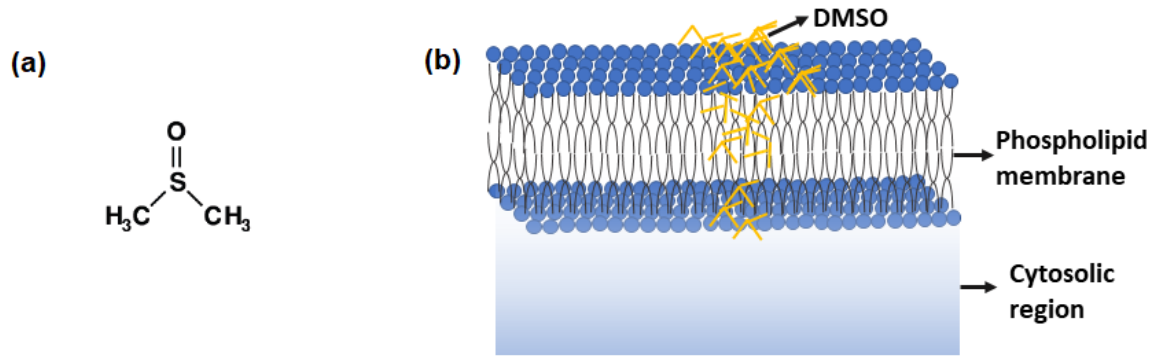

Figure 4.7: Effect of DMSO on the phospholipid membrane of cells: (a) Chemical structure of dimethyl sulfoxide. (b) Schematic diagram to explain the permeability of DMSO through the phospholipid membrane and penetrating through the lipid bilayer to the cytosolic region.

DMSO thins membranes and increases the fluidity of the membrane's hydrophobic core at low concentrations ($< 0.5\% < 1\%$). DMSO causes transitory water holes in the membrane at higher concentrations ($> 1\%$). At even higher concentrations, the lipid molecules are removed from the surface of the membrane which results in the disintegration of the lipid bilayer [Gurtovenko and Anwar, 2007]. We focus here on monitoring the effect of DMSO on the membrane permeability of the 8-FDA-cAMP molecules on HEK cells was observed by experimental analysis. FDA was used as a control for the experiment. The fluorescence intensity was recorded for the cellular uptake kinetics of FDA analogs in HEK293T cells with increasing concentration DMSO. The Neo2 plate reader (Synergy Neo2 Hybrid Multi-Mode Reader) was employed for the measurement of fluorescence intensities within cells populations.

The fluorescence intensity was recorded for the cellular uptake of the FDA molecule on HEK293T cells with increasing concentrations of DMSO. The Clear Bottom Polymer Base 96-Well Plates (Thermo Scientific™) were used for this experiment. The HEK293T cells were cultured in a 96-well plate with DMEM culture medium (Glucose, Sodium pyruvate, L-Glutamate and $NaHCO_3$) and one row was kept empty for measuring background. The cells were cleaned twice with an HBSS medium before the experiment. Then added FDA (1 µM) with increasing concentrations of 0.01, 0.05, 0.1, 0.5, 1 & 5 mol $\%$ of DMSO in HBSS ($+CaCl_2 + MgCl_2$) buffer. For measuring background noise, one row of the 96-well plate was filled with HBSS buffer with an increasing concentration of DMSO. The fluorescence intensity for the cellular uptake of FDA in a microplate reader was obtained at an excitation of 488 nm and emission at 520 nm at 37 $^{\circ}C$. After obtaining the uptake data, the background was subtracted and plotted the cel-

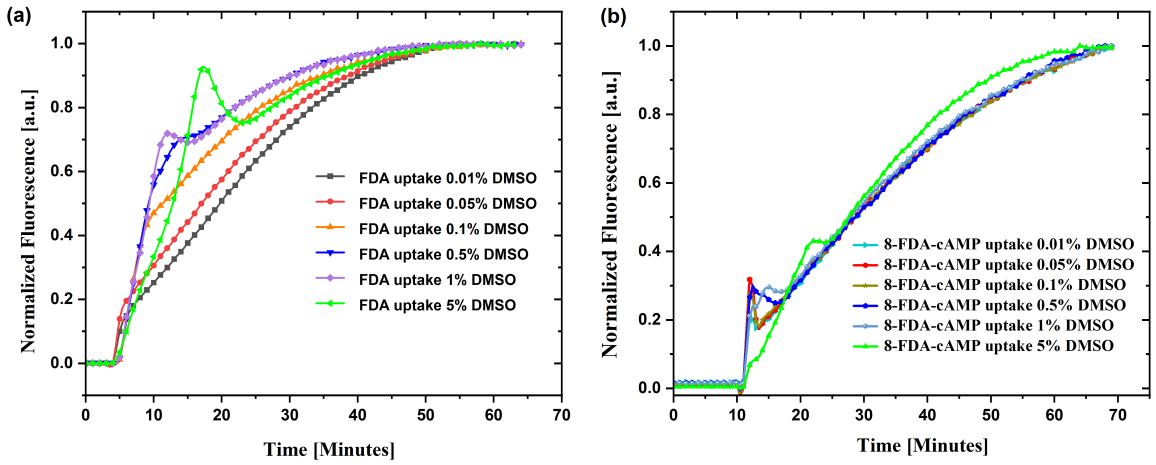

Figure 4.8: Cellular uptake kinetics of FDA & 8-FDA-cAMP in a microplate reader at excitation of 488 nm and emission at 520 nm on HEK293T cells: Cellular uptake kinetics of (a) FDA (C = 1 µM) and (b) 8-FDA-cAMP (C = 10 µM) with increasing concentration 0.01, 0.05, 0.1, 0.5, 1 & 5 mol % of DMSO. The KEK293T cells are used for the experiment with the imaging medium of HBSS ($+CaCl_2 + MgCl_2$) incubated at 37 $^{\circ}C$ on 96 well plate. Each data points on the uptake kinetics curve represent the real-time mean normalized intensities of the drug uptake into the cell measured by microplate reader. To get the control for this experiment, the uptake kinetics for FDA and 8-FDA-cAMP were performed in a single raw 96-well plate in HBSS buffer with increasing DMSO concentration without cells.

lular uptake data of FDA (Figure 4.8 a) with time points. From the cellular uptake plot of FDA (Figure 4.8 a), it can be observed that the behaviour of the uptake changes with increasing the percentage of DMSO concentration. With the increase of % mol of DMSO, the uptake kinetics becomes faster and up to 0.5 mol % of DMSO in the medium, the behaviour of the uptake remains almost similar as discussed earlier [Gurtovenko and Anwar, 2007].

With the increasing % mol of DMSO ($> 0.5\%$), there was a substantial peak observed in the uptake kinetics of FDA for HEK293T cells. The kinetics of the uptake became faster with the increasing concentration of DMSO and at 5 mol % DMSO concentration, a dramatic change in the uptake curve was observed. Our initial assumption for such uptake was due to pore formation in the membrane, since molecular dynamics simulations have shown that DMSO can create pores in the phospholipid bilayer [Notman et al., 2006]. With the increase of DMSO concentration, the membrane becomes floppier which enhances the permeability of the drug through the membrane [Notman et al., 2006]. For further increase in concentration ($> 0.5\%$) which implies the osmotic and mechanical stress on the membrane breaks the lipid bilayer.

DMSO concentration	Saturation time T_1 (Minutes)	Saturation time T_2 (Minutes)
0.01% DMSO	36.2 ± 2.4	36.2 ± 4.4
0.05% DMSO	24.2 ± 2.3	24.3 ± 2.6
0.1% DMSO	1.5 ± 0.2	17.6 ± 0.5
0.5% DMSO	1.9 ± 0.3	16.8 ± 1.8
1% DMSO	1.8 ± 0.5	14.6 ± 2.1
5% DMSO	1.4 ± 0.3	11.5 ± 1.3

Table 4.1: Table for the measurement of saturation time of FDA uptake on HEK293T cells with the increasing concentration of DMSO.

The rate of uptake of FDA corresponding to each concentration of DMSO obtained by fitting the uptake curve with the double exponential growth function;

$$Y = A_1\, e^{\frac{X}{T_1}} + A_2\, e^{\frac{X}{T_2}} + Y_0$$

Where, T_1 and T_2 correspond to the saturation times for the uptake kinetics of drug analogues, as extracted from double exponential fit. The saturation time for different DMSO concentrations were obtained by double exponential growth function as given in the Table 4.1. From the table, it can be observed that with the increase of DMSO percentage in the imaging environment the corresponding saturation time for the uptake kinetics of FDA decreases. By referring to our hypothesis that DMSO causes membrane permeability, it may be deduced that DMSO causes the membrane flexibility, resulting in quicker drug permeability with more its concentration outside the lipid bilayer.

As previously stated, DMSO acts as a cargo carrier for drug and DNA membrane permeability [de Ménorval et al., 2012]. In Section 4.1, we discussed the cellular uptake kinetics of the 8-FDA-cAMP molecule. From the cellular uptake kinetics of drug analogues, it was observed that the 8-FDA-cAMP molecule becomes increasingly permeable into the cell with the increase in DMSO concentration. Certain drugs or large peptides unable to permit the lipid bilayer, so DMSO acted as a promoter to make those compounds permeable into the cellular environment. In this section, the permeability of FDA's membrane at various DMSO molar concentrations was explored.

Temperature is also known to play a key role in the uptake kinetics of drugs across the lipid bilayer. The objective of this work was to observe the cellular uptake of FDA at 0.5 mol$\%$ DMSO and at different

temperatures. The uptake of FDA into the HEK293T cells was obtained at three different temperatures (20 $°C$, 30 $°C$ & 30 $°C$). From Figure 4.9, it can be observed that the cellular uptake kinetics of FDA at 0.5 mol % DMSO concentration at different temperatures. With the increased temperature of environment, the uptake kinetics was faster at the same DMSO concentration (Figure 4.9). The comparison of the uptake kinetics of FDA and 8-FDA-cAMP molecules with different DMSO concentrations is shown in Figure 4.10. The intensity for the uptake of FDA and 8-FDA-cAMP molecules were normalized to a same scale. It can be observed from the Figure (4.10) that the behaviour of uptake kinetics of both compounds with the increasing DMSO concentration was similar, whereas the uptake kinetics of FDA was faster than that of 8-FDA-cAMP.

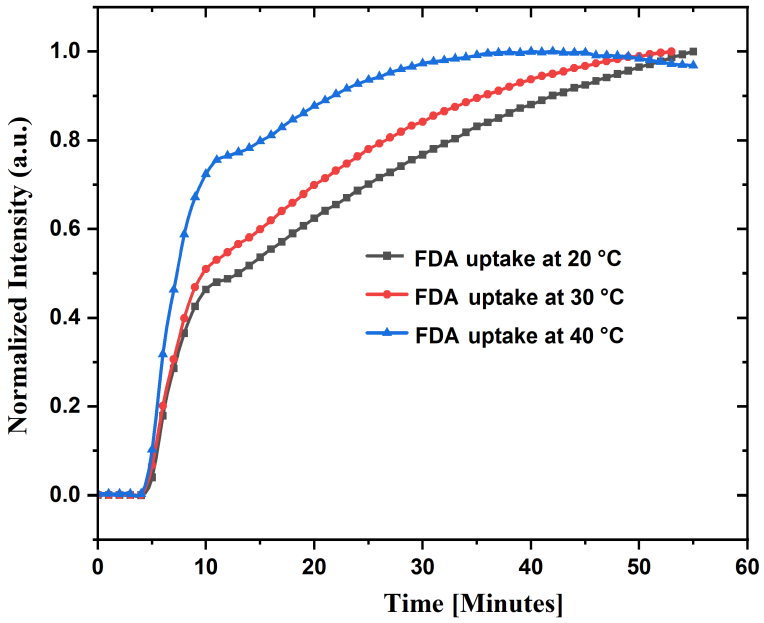

Figure 4.9: Temperature dependent cellular uptake kinetics of FDA molecule in a microplate reader at excitation of 488 nm and emission at 520 nm on HEK293T cells: Temperature dependent Cellular uptake kinetics of FDA of 1 µM at 0.05% mol DMSO on HEK293T cells in HBSS buffer at pH 7.3.

The effect of DMSO in a phospholipid membrane on liquid-crystalline phase was systematically studied by Gurtovenko et al. [Gurtovenko and Anwar, 2007]. They employed the atomic-scale molecular dynamics simulations at realistic potentials to observe the permeability of DMSO into the membrane. The 14 different concentrations of DMSO were studied with varying concentrations of 0 mol % to 100 mol %. The effect of DMSO on phospholipid membranes is summarized in the Figure 4.11. The effect of DMSO at 4 distinct concentrations on the membrane permeability was studied in the molecular dynamics simulation. According to this study, at (2.5–7.5 mol %) of DMSO the thickness of the membrane

decreases, transient water pore induced (10–70 mol %) and the bilayer structure of the membrane are destroyed at (25–100 mol %) of DMSO. The characteristics of the pore formation features were found to be strongly dependent on the DMSO concentration. Although, a similar behaviour was experimentally observed for the uptake kinetics of FDA and 8-FDA-cAMP molecule on HEK293T cells, however, the concentration dependence of DMSO for the membrane permeability of HEK293T cells was found to be different.

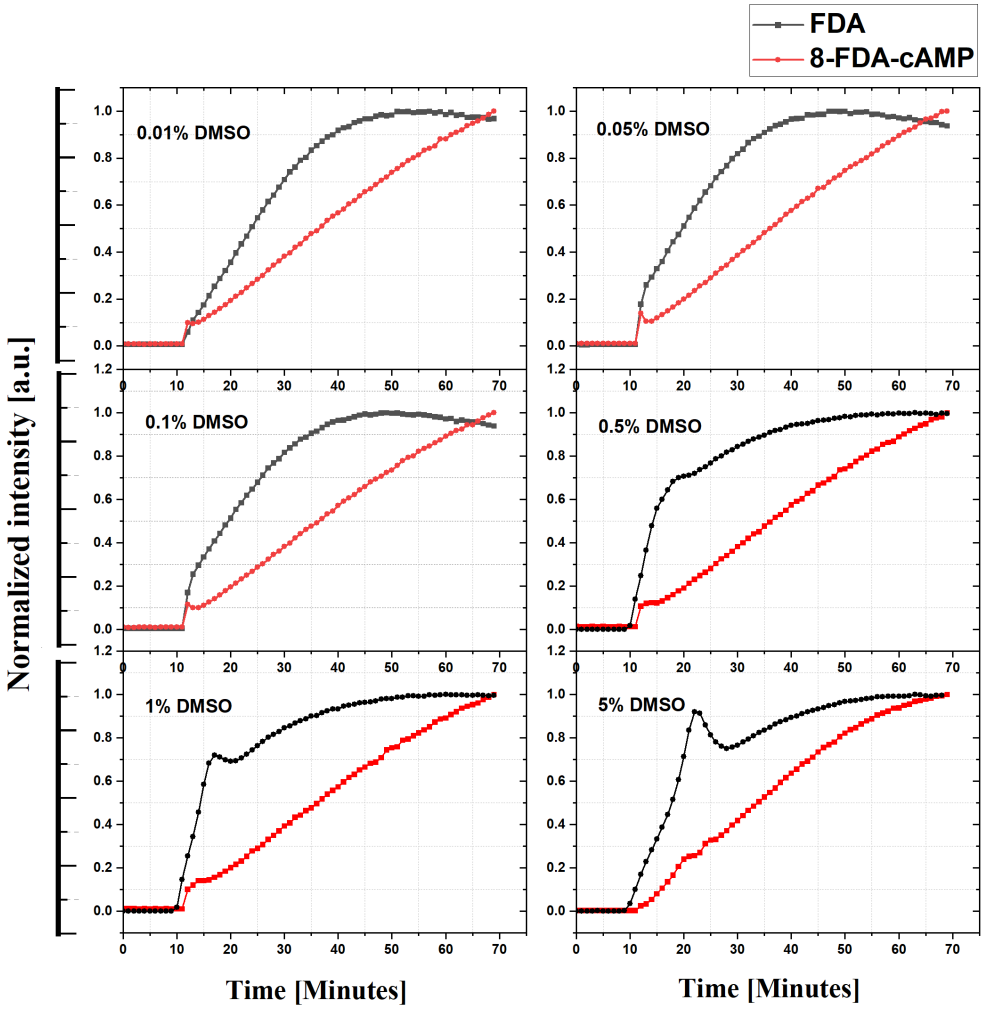

Figure 4.10: Comparison of the uptake kinetics plot of FDA (1 μM) and 8-FDA-cAMP (10 μM) with increasing concentration 0.01, 0.05, 0.1, 0.5, 1 & 5 mol % of DMSO. The HEK293T cells are used for the experiment with the imaging medium of HBSS ($+CaCl_2 + MgCl_2$) incubated at 37 °C temperature on 96 wall plate. Each data points on the uptake kinetics curve represent the real-time mean normalized intensities of the drug uptake into the cell measured by a microplate reader.

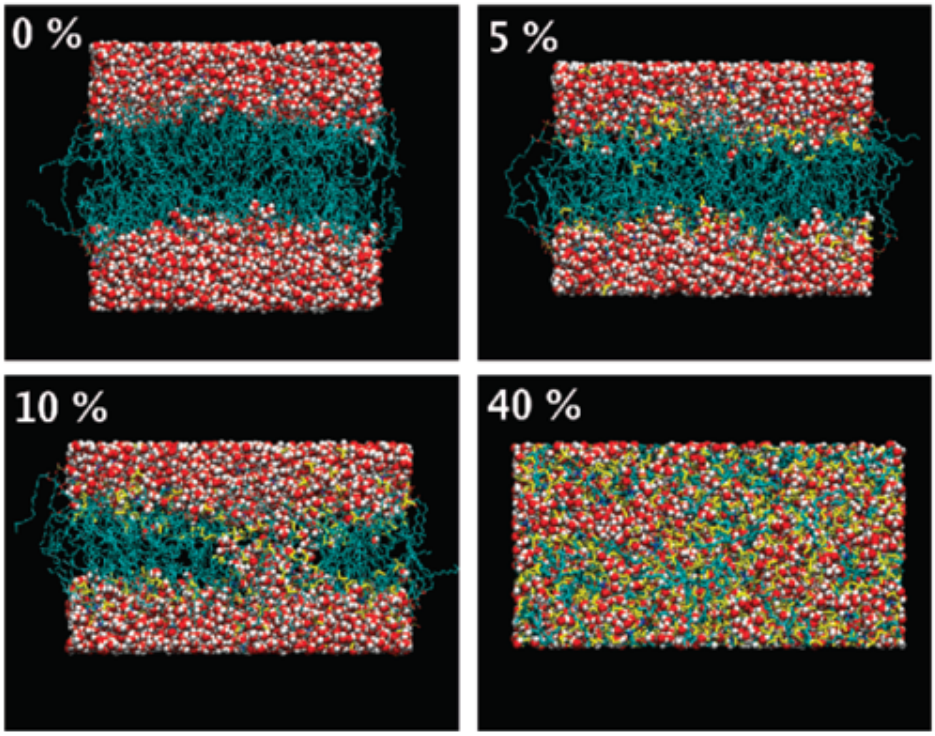

Figure 4.11: Effect of DMSO on membrane permeability obtained by molecular dynamics simulations: Effect of DMSO on phospholipid membranes. This figure contains the structure of bilayer containing different percentage of DMSO (0%, 5%, 10% & 40%) . Lipids are shown in cyan, water in red and DMSO in yellow [Gurtovenko and Anwar, 2007]

In Summary, from the experimental work we obtained the cellular uptake kinetics of 8-FDA-cAMP molecule (10 μM) with increasing concentrations of 0.01, 0.05, 0.1, 0.5, 1 & 5 mol % of DMSO on HEK293T cells. The uptake kinetic data were obtained for the 8-FDA-cAMP molecule and after subtracting the background the data was plotted with time points as shown in Figure 4.8 (b). A similar pattern was observed for the uptake kinetics of 8-FDA-cAMP molecules to that of FDA. Below 1% mol DMSO concentration the uptake kinetics were almost similar, however, we hypothesize that the increase in the DMSO concentration resulted in pores in the lipid bilayer [Gurtovenko and Anwar, 2007]. From the comparison of our findings with the computational results there was a similar behaviour obtained for the DMSO permeability into the membrane, however, the concentration was different. As a result, the variation in concentration was caused by the experiment's use of various cell lines. The most significant findings of our experimental work was the DMSO making transient pore in the membrane at higher concentration, similar to the findings observed in coarse-grained simulations. Finally, this study emphasizes the importance of selecting the optimal concentration of DMSO for penetrating large drugs and peptides into the cytosolic region in cellular experiments.

Chapter 5

Conclusion and outlook

Fluorescence spectroscopy and microscopy are an essential part for the characterization of novel fluorescent based drug analogues. We employed advanced fluorescent spectroscopy and microscopy techniques to characterize three novel fluorescent drug analogues in terms of fluorescent properties and cellular uptake. The TCSPC experimental setup was employed for the measurement of spectral properties due to its high sensitivity detection system and the measurement of lifetime with greater accuracy. The instrument response function (IRF) and the sensitivity of photon counting in the detector were optimized for the TCSPC instrument.

By taking fluorescein diacetate (FDA) as a reference, the spectra, absorbance, fluorescence intensity and fluorescence lifetime of the drug analogues (8-FDA-cAMP, MAN193 & AG3457) are characterized as represented in Table 3.3. The outcome from the measurement of absorbance of 8-FDA-cAMP (Dark state) lead to the conclusion that the part of 8-FDA-cAMP molecule were in pre-activated state. A significantly lower fluorescence intensity is obtained for MAN194 and 8-F-cAMP molecule, which suggests the lower quantum yield of this molecule as compare to that of fluorescein. We conclude from the experimental results that the quantum yield of the fluorescein compound is higher than the AG3457-activated molecule; however, the quantum yield of MAN194 & 8-F-cAMP are very low with respect to the AG3457-activated molecule. The results from saturation binding assays indicates that the MAN194 molecule is binding to the associated purified protein and the dissociation binding parameter obtained by the sigmodial function fit. We have not succeeded in observing binding AG3457-activated molecule with the target proteins and this would require further modification and experimental studies for future

applications.

The behaviour of fluorescent drug analogues in the intracellular environment was measured by laser scanning confocal microscopy. The cellular import kinetics of fluorescence drug analogues inside the HEK293T cells are observed with the confocal microscopy images. The outcome of various cellular uptake experiments leads to the conclusion that the subcellular localization of drugs in the mitochondrial region is observed for fluorescein, 8-FDA-cAMP and MAN193 molecule. However, no subcellular localization is observed in the case of AG3457 molecule. The results of the competition binding experiment for MAN193 and 8-FDA-cAMP molecule conclude the co-localization and uptake of drug analogues in the perimitochondrial region of cells. Our measurements could not provide a molecular identity for the putative binding sites, and a superresolution imaging strategy would be needed to begin addressing this question in living cells. Future work may focus on the cellular uptake kinetics for different cell lines using high-resolution expansion microscopy set up to observe the specific binding sites of the drug analogues in the mitochondrial region. Finally, we studied the effect of dimethyl sulfoxide (DMSO) on the membrane permeability of 8-FDA-cAMP molecules at different concentrations. From various fluorescent spectroscopy and cellular uptake experiments, the concentration of 0.05 mol $\%$ of DMSO was identified to be most suitable for the cellular uptake experiments. The results from our study and published data support the conclusion that the effect of DMSO makes the lipid bilayer flexible which results in the increased permeability of larger drug analogues. However, the further increase in the concentration of DMSO ($\sim 5\%$) results in pores in the lipid bilayer.

Bibliography

[Bock et al., 2020] Bock, A., Annibale, P., Konrad, C., Sivaramakrishna, S., Falcke, M., and J. Lohse, M. (2020). Optical mapping of camp signaling at the nanometer scale. *Cell*, 182:1519–1530.

[de Ménorval et al., 2012] de Ménorval, M.-A., M Mir, L., Fernández, M. L., and Reigada, R. (2012). Effects of dimethyl sulfoxide in cholesterol-containing lipid membranes: A comparative study of experiments in silico and with cells. *PLoS ONE*, 7:1932–6203.

[Engelborghs and Visser, 2014] Engelborghs, Y. and Visser, A. J. (2014). Fluorescence spectroscopy and microscopy. *Methods in Molecular Biology*, 1076(3745):XXI–816.

[Gironi et al., 2020] Gironi, B., Kahveci, Z., McGill, B., Lechner, B.-D., Pagliara, S., Metz, J., Morresi, A., Palombo, F., Sassi, P., and Petrov, P. G. (2020). Effect of dmso on the mechanical and structural properties of model and biological membranes. *Biophysical Journal*, 119:274–286.

[Gurtovenko and Anwar, 2007] Gurtovenko, A. A. and Anwar, J. (2007). Modulating the structure and properties of cell membranes: The molecular mechanism of action of dimethyl sulfoxide. *J. Phys. Chem. B*, 111:10453–10460.

[Herschel, 1845] Herschel, J. F. W. (1845). On a case of superficial colour presented by a homogeneous liquid. *Philosophical Transactions of the Royal Society of London*, 135:143–145.

[Horiba, 2009] Horiba, S. (2009). A practical guide to time-resolved luminescence lifetime determination using dedicated time-correlated single photon counting systems. *Technical Report*, pages 1–31.

[Hwang et al., 2021] Hwang, W., Kim, D., Moon, S., and Kim, D. Y. (2021). Achieving a high photon count rate in digital time-correlated single photon counting using a hybrid photodetector. *Optics Express*, 29:9797—-9804.

[Jokic et al., 2012] Jokic, T., Borisov, S. M., Saf, R., Nielsen, D. A., Kuhl, M., and Ingo Klima (2012). Highly photostable near-infrared fluorescent ph indicators and sensors based on bf2-chelated tetraarylazadipyrromethene dyes. *Anal. Chemistry*, 82:6723–6730.

[Klarenbeek et al., 2015] Klarenbeek, J., Goedhart, J., van Batenburg, A., Groenewald, D., and Jalink, K. (2015). Fourth-generation epac-based fret sensors for camp feature exceptional brightness, photostability and dynamic range:characterization of dedicated sensors for flim, for ratiometry and with high affinity. *The Journal of Physical Chemistry B*, 1371:1—-11.

[Kuleshova et al., 2014] Kuleshova, L. G., Gordienko, E. A., and Kovalenko, I. F. (2014). Permeability of isolated rat hepatocyte plasma membranes for molecules of dimethyl sulfoxide. *Biophysics*, 59:387–392.

[Laine, 2013] Laine, R. (2013). Fluorescence lifetime spectroscopy and imaging of fret probes for the study of cell signaling. *PhD Thesis, Imperial College London*, pages 1–292.

[Lakowicz, 2006a] Lakowicz, J. R. (2006a). Chapter 1: Introduction to fluorescence, principles of fluorescence spectroscopy. *Springer US*, pages 1–25.

[Lakowicz, 2006b] Lakowicz, J. R. (2006b). Chapter 10: Fluorescence anisotropy, principles of fluorescence spectroscopy. *Springer US*, pages 353–381.

[Lakowicz, 2006c] Lakowicz, J. R. (2006c). Chapter 2: Instrumentation for fluorescence spectroscopy, principles of fluorescence spectroscopy. *Springer US*, pages 27–60.

[Lakowicz, 2006d] Lakowicz, J. R. (2006d). Chapter 4: Time-domain lifetime measurements, principles of fluorescence spectroscopy. *Springer US*, pages 98–154.

[Laskaratou et al., 2021] Laskaratou, D., Fernández, G. S., Coucke, Q., Fron, E., Rocha, S., Hofkens, J., Hendrix, J., and Mizuno, H. (2021). Quantification of fret-induced angular displacement by monitoring sensitized acceptor anisotropy using a dim fluorescent donor. *Nature Comunications*, 12(2541):1–12.

[Lee et al., 2011] Lee, J. S., Koehorst, R. B. M., and van Amerongen, H. (2011). Time-resolved fluorescence and fluorescence anisotropy of fluorescein-labeled poly(n-isopropylacrylamide) incorporated in polymersomes. *The Journal of Physical Chemistry B*, 115:13162—-13167.

[Murphy and Davidson, 2012] Murphy, D. B. and Davidson, M. W. (2012). Fundamentals of light microscopy and electronic imaging. *Wiley Online Library*, 118:265–355.

[Notman et al., 2006] Notman, R., Noro, M., O'Malley, B., and Anwar, J. (2006). Molecular basis for dimethylsulfoxide (dmso) action on lipid membranes. *Journal of the American Chemical Society*, 43:13982–13983.

[Sauer et al., 2011] Sauer, M., Hofkens, J., and Enderlein, J. (2011). Handbook of fluorescence spectroscopy and imaging. *Wiley-VCH Verlag GmbH Co. KGaA*, pages 01–29.

[Sjöback et al., 1995] Sjöback, R., Nygren, J., and Kubista, M. (1995). Absorption and fluorescence properties of fluorescein. *Spectrochimica Acta Part A*, 51:L7–L21.

[Teijeiro-Gonzalez et al., 2020] Teijeiro-Gonzalez, Y., Crnjar, A., Beavil, A. J., Beavil, R. L., Nedbal, J., Marois, A. L., Molteni, C., and Suhling, K. (2020). Time-resolved fluorescence anisotropy and molecular dynamics analysis of a novel gfp homo-fret dimer. *Biophysical Journal*, 120:254–269.

[Valeur, 2001] Valeur, B. (2001). Molecular fluorescence: Principles and applications. *Wiley-VCH Verlag GmbH Co. KGaA*, pages 20–33.

[Wahl, 2014] Wahl, M. (2014). Time correlated single photon counting (tcspc). *Technical Report*, pages 1–14.

[Wahl and Orthaus-Müller, 2014] Wahl, M. and Orthaus-Müller, S. (2014). Time tagged time-resolved fluorescence data collection in life sciences. *Technical Report*, pages 1–10.

[Wang et al., 2010] Wang, H., Zhong, C.-Y., Wu, J.-F., Huang, Y.-B., and Liu, C.-B. (2010). Enhancement of tat cell membrane penetration efficiency by dimethyl sulphoxide. *Journal of Controlled Release*, 143:64–70.

[Yu and Quinn, 1998] Yu, Z.-W. and Quinn, P. J. (1998). The modulation of membrane structure and stability by dimethyl sulphoxide (review). *Molecular Membrane Biology*, 15:59–69.

[Yu and Quinn la, 1994] Yu, Z.-W. and Quinn la, P. J. (1994). Dimethyl sulphoxide: A review of applications in cell biology. *Bioscience Reports*, 14:259–281.

[Zhang et al., 2014] Zhang, X.-F., Zhang, J., and Liu, L. (2014). Fluorescence properties of twenty fluorescein derivatives: Lifetime, quantum yield, absorption and emission spectra. *Journal of Fluorescence*, 24:819–826.

[Zhong, 2009] Zhong, W. (2009). Nanomaterials in fluorescence-based biosensing. *Analytical and Bioanalytical Chemistry*, 394:47–59.

Declaration of Authorship

I, Jagannath Satpathy, declare that this thesis and the work presented in it is my own.

This work was completed while in candidature for a master's degree in Physics at the Freie Universität Berlin. I have explicitly marked all material which has been quoted either literally or by content from the used sources.

Date: July 6, 2022

Signature: _____

Jagannath Satpathy